FEDERAL UNIVERSITY OF SANTA CATARINA
TECHNOLOGY CENTER
AUTOMATION AND SYSTEMS DEPARTMENT
UNDERGRADUATE COURSE IN CONTROL AND AUTOMATION ENGINEERING

Pollyana Gomes Minatel

Predicting Workpiece Deformation Using Thermogrammetry-Based Finite Element Analysis

Aachen
2023

Pollyana Gomes Minatel

Predicting Workpiece Deformation Using Thermogrammetry-Based Finite Element Analysis

Final report of the subject DAS5511 (Course Final Project) as a Concluding Dissertation of the Undergraduate Course in Control and Automation Engineering of the Federal University of Santa Catarina.
Advisor Prof. Hector Bessa Silveira, Dr.
Supervisor Dominik Emonts, Eng.

Aachen
2023

Ficha de identificação da obra elaborada pelo autor,
através do Programa de Geração Automática da Biblioteca Universitária da UFSC.

Minatel, Pollyana Gomes
Predicting workpiece deformation using thermogrammetry based finite element analysis / Pollyana Gomes Minatel ; orientador, Hector Bessa Silveira, coorientador, Dominik Emonts, 2023.
81 p.

Trabalho de Conclusão de Curso (graduação) - Universidade Federal de Santa Catarina, Centro Tecnológico, Graduação em Engenharia de Controle e Automação, Florianópolis, 2023.

Inclui referências.

1. Engenharia de Controle e Automação. 2. Finite element method. 3. Digital twin. 4. Workpiece. 5. Thermoelastic deformation. I. Silveira, Hector Bessa. II. Emonts, Dominik. III. Universidade Federal de Santa Catarina. Graduação em Engenharia de Controle e Automação. IV. Título.

Pollyana Gomes Minatel

Predicting Workpiece Deformation Using Thermogrammetry-Based Finite Element Analysis

This dissertation was evaluated in the context of the subject DAS5511 (Course Final Project) and approved in its final form by the Undergraduate Course in Control and Automation Engineering

Florianópolis, February 28, 2023.

Prof. Hector Bessa Silveira, Dr.
Course Coordinator

Examining Board:

Prof. Hector Bessa Silveira, Dr.
Advisor
UFSC/CTC/DAS

Dominik Emonts, Eng.
Supervisor
WZL - RWTH Aachen University

Prof. Laio Oriel Seman, Dr.
Evaluator
UFSC/CTC/DAS

Prof. Eduardo Camponogara, Dr.
Board President
UFSC/CTC/DAS

This work is dedicated to my family who supported me
and encouraged me to keep going during all the
challenges of this work.

ACKNOWLEDGEMENTS

Firstly, I am grateful to my family for all the support that has been given to me during this adventure. I thank my boyfriend, who embarked with me on the big changes that were necessary, including living in Germany, and did not spare any effort to always support me. I thank my academic advisor, Hector, for the support that guided me to overcome many challenges during this project. His accompaniment was essential and will always be remembered. Thank you for being such an inspiring teacher. Thanks to my supervisor at the company, Dominik Emonts, who patiently guided me through the entire development of this project. I admire all the time dedicated in this work. Know that you were essential for me to achieve this result. I would also like to thank Jan-Henrik who worked alongside me and was extremely important to my learning process. I thank the Brazilian National Petroleum Agency (ANP) for the in-depth training in the area of oil and gas, for the scholarship, and for the research project that I was able to develop during my period in the PRH-ANP program. All the knowledge acquired was extremely important to get where I am now. I am grateful for the financial support from the Human Resources Program of the National Agency of Petroleum, Natural Gas and Biofuels - PRH-ANP, supported with resources from the investment from oil companies qualified in the R, DI Clause of ANP Resolution No. 50/2015. I also thank my advisor at PRH-ANP who was very patient and taught me a lot during the project. He was also essential for me to be able to develop this thesis in another country and fulfill a great dream. Lastly, but not less important, I thank the Universidade Federal de Santa Catarina and all the professors who were with me on this journey for giving me the resources and knowledge necessary for me to graduate as a control and automation engineer.

ABSTRACT

Work-pieces are subject to significant thermoelastic effects, or expansion in size. when exposed to transient temporal thermal conditions. Manufacturing, assembly, and measurement errors may arise as a result of this issue, particularly for large workpieces such as turbine housings used in power plants. For this reason, the capability to predict deformations in the object structure, specially for ones with non-trivial shapes, is needed. The aim of this work is to develop a virtual climatization methodology, using many measurement tools, to analyze and predict workpiece deformations based on its acquired temperature. The prediction is necessary in order to compensate the thermoelastic deformation, which is the physical event of the material change in size due to temperature variation. This result was achieved by carrying out an experiment in which a turbine housing was purposely heated for 3 hours, while various measurement tools were monitoring the object: a laser tracker measured the physical deformations of the workpiece, while surface temperature sensors and a thermal camera monitored its temperature. The sensors measured the temperature at some points, while the rest of it was covered by the camera. The temperature data was converted from 2D to 3D by using UV mapping, in which the 2D thermal image was attached to a virtual 3D object. Further manipulations such as data treatment and interpolation were applied. The interpolation technique was implemented with Ordinary Kriging and Dijkstra's algorithm to improve the temperature distribution in the workpiece. Then, a finite element method (FEM) simulation was performed using a digital thermal twin of the workpiece. Such digital twin was obtained based on the acquired temperature data from the experiment and on the construction of a 3D model of the turbine housing. To improve accuracy and distribution of temperature through the whole object, an interpolation technique using the known temperature values was implemented. The FEM simulation allowed a better understanding of the thermoelastic behavior of the workpiece under different temperature ranges. Its result was compared to the data of the real measurement of the object's expansion, showing that the FEM simulator can provide a predicted expansion with an average error of 8.73% relative to the linear temperature expansion theoretical values. The analysis of the results showed that the developed technique is very sensitive to small changes in the used variables and parameters, especially in the interpolation step, which can strongly influence the final result. Various possible sources of such sensibility were determined, so that they can be further explored in future investigations.

Keywords: Finite element method. Digital twin. Interpolation. Workpiece. Thermoelastic deformation.

RESUMO

Objetos no geral estão sujeitos a efeitos termoelásticos, ou expansão em tamanho, significativos quando expostos a condições térmicas temporais transitórias. Como resultado desta questão, podem surgir erros de fabricação, montagem e medição, principlamente para peças de grande porte, como carcaças de turbinas usadas em usinas de energia. Por este motivo, é necessária a capacidade de prever deformações na estrutura do objeto, especialmente aquelas com formatos não triviais. O objetivo deste trabalho é desenvolver uma metodologia de climatização virtual, utilizando múltiplas ferramentas de medição, para analisar e predizer deformações nas peças com base nos dados de temperatura adquiridos. A predição é necessária a fim de compensar a deformação termo-elástica, que é a mudança de tamanho do material devido à variação de temperatura. Este resultado foi alcançado através da realização de um experimento no qual uma carcaça de turbina foi intencionalmente aquecida durante 3 horas, enquanto várias ferramentas de medição monitoravam o objeto: um rastreador a laser media as deformações físicas da peça de trabalho, enquanto sensores de temperatura superficial e uma câmera térmica monitoravam sua temperatura. Os sensores mediam a temperatura em alguns pontos, enquanto o resto era coberto pela câmera. Os dados de temperatura foram convertidos de 2D para 3D usando o mapeamento UV, no qual a imagem térmica 2D foi anexada a um objeto virtual 3D. Outras manipulações, como tratamento de dados e interpolação, foram aplicadas. A técnica de interpolação foi implementada com *Ordinary Kriging* e o algoritmo de Dijkstra para melhorar a distribuição da temperatura no objeto virtual. Em seguida, foi realizada uma simulação de elementos finitos (FEM) usando um gêmeo térmico digital da carcaça de turbina. Tal gêmeo digital foi obtido com base nos dados de temperatura adquiridos no experimento e na construção de um modelo 3D da carcaça da turbina. Para melhorar a precisão e distribuição da temperatura através de todo o objeto, foi implementada uma técnica de interpolação usando os valores de temperatura conhecidos. A simulação FEM permitiu uma melhor compreensão do comportamento termoelástico da peça de trabalho sob diferentes faixas de temperatura. Seu resultado foi comparado aos dados da medição real da expansão do objeto, mostrando que o simulador FEM pode fornecer uma expansão prevista com um erro médio de 8,73% em relação aos valores teóricos da expansão linear de temperatura. A análise dos resultados mostrou que a técnica desenvolvida é muito sensível a pequenas mudanças nas variáveis e parâmetros utilizados, especialmente na etapa de interpolação, o que pode influenciar fortemente o resultado final. Várias possíveis fontes de tal sensibilidade foram expostas para que possam ser mais exploradas em investigações futuras.

Palavras-chave: Finite element method. Digital twin. Interpolation. Work-piece. Thermoelastic deformation.

LIST OF FIGURES

LIST OF TABLES

LIST OF ABBREVIATIONS AND ACRONYMS

2D	2 Dimensional
3D	3 Dimensional
CTE	Coefficient of Thermal Expansion
DTT	Digital Thermal Twin
FEM	Finite Element Method
IDE	Integrated Development Environment
LSM	Large Scale Metrology
LTE	Linear Thermal Expansion
M.O.D.	Minimum Distance of Object
RGB	Red, Green, Blue
RWTH	Rhenish-Westphalian Technical University
SMR	Spherically Mounted Retroreflector
WZL	Werkzeugmaschinenlabor

CONTENTS

1 INTRODUCTION

Fluctuations in the temperature of large workpieces in industrial fields may result in multiple issues, including diminished product quality and efficiency due to thermoelastic deformations on the physical dimensions of the object. Industries that manufacture components and objects for energy production, such as gas turbines and their housing, are particularly susceptible to the consequences of thermal variations, such as vulnerabilities in safety and negative financial impacts.

The heterogeneity of an object's temperature in time results in an expansion or contraction of the object's material, which causes it to have a different size proportional to the change. This behavior is known as the thermo-elastic deformation of a material and is a consequence of the agitation level of the molecules. In case of an increase in temperature, the molecules became agitated and there is a visible physical expansion of the object.This event can happen in different levels in the same object if its temperature is heterogeneous.

Despite the fact that the properties of the material of an object exert a significant influence on its thermoelastic behavior, that is, its expansion or contraction as a consequence of its temperature, parameters of the surrounding environment also impact the object's behavior, such as the ambient temperature or airflow. These factors must be taken into consideration during the production processes of a large workpiece, as even the manufacturing process of the object can heat the material and cause a temporary, as well as permanent, change in its size, which can result in potential production errors.

Virtual climatization is a technology that combines sensors, models, and data processing to allow the creation of a methodology or technique to compensate any change. In the energy industry, the compensation of thermoelastic deformation using virtual climatization may result in a reduction of energy consumption, improvement of the quality control cycle, and reduction of measurement uncertainty.

Considering how important the temperature fluctuation of an object is in its production environment, it is necessary to understand how the large-scale object behaves with these changes since it is unlikely to have a homogeneous temperature throughout its entire spacial distribution. For this reason, this project focuses on the study of the virtual climatization of large components looking for a possibility of compensating any thermal changes that may impact the object.

This work was developed in the Laboratory for Machine Tools and Production Engineering, also known as Werkzeugmaschinenlabor (WZL), which is part of the Rhenish-Westphalian Technical University (RWTH) Aachen University, located in Aachen, Germany. The institute conducts research focused on development about relevant engineering areas and innovative subjects. The specific sector in which this work was studied is focused on production metrology and quality management, including

virtual climatization.

While the topics studied in WZL within virtual climatization are many, such as automatic communication interface for On-Demand sensor, remote environmental monitoring and machine production monitoring, one of the projects has a goal of study large workpieces and its temperature during the manufacturing process. This specific project inspired this work, since the study of virtual climatization for large workpieces can have a positive impact in the quality and costs of production and efficiency of the final product.

Within the virtual climatization, more specific areas were addressed in this work. With the goal of creating a methodology to predict and compensate thermo-elastic deformation in large workpieces production, such as a turbine housing, different measuring tools were used to monitor the turbine housing in different temperature conditions for several consecutive hours.

To achieve the stated goal, the proposed solution concerns the use of data regarding the temperature and spacial distribution of the workpiece to create a virtual object similar to the real one. This virtual object allows a more in-depth analysis of its thermo-elastic behavior and simulations in order to predict the object deformation under different conditions.

By intentionally heating up a turbine housing and monitoring its thermoelastic behavior with temperature sensors, a thermography and RGB cameras, and a laser tracker capable of detecting slight changes in distances, thermal and expansion data were acquired and processed for a better understanding of the expansion pattern in the whole object.

While temperature sensors acquired data from specific points of the turbine, the thermal camera acquired temperature from the whole workpiece in its visual field. Since the sensors have a better accuracy than the camera, their data was used to calibrated the images. Both sources of data were transformed from a 2 Dimensional (2D) plane to a 3 Dimensional (3D) using UV-mapping technology, which resulted in the attachment of temperature from the real object to the virtual one. Then, to improve the temperature distribution in the whole workpiece, an interpolation was performed.

The collected and processed data was used to create a digital thermal twin of the object, which was later used for finite element method (Finite Element Method (FEM)) simulation in an attempt to predict the object's behavior under different temperature conditions. A comparison between the simulation results and real measurements, with the data acquired with the laser tracker, was performed to verify the simulation accuracy and also narrow down possible sources of error during the data acquisition and processing.

The necessity of a prediction tool using cameras and simulation exists due to limitations of the laser tracker. The laser can only measure specific points that have Spher-

ically Mounted Retro-reflectors (Spherically Mounted Retroreflector (SMR)s), since its functionality depends on the reflection of the pointed laser to the equipment, which uses the time delay to calculate the distance from the equipment to the mirror target. Despite the great accuracy provided, the laser is limited to a number of points, while the rest of the workpiece is not measured. More over, a methodology that uses a 3D realistic virtual object and simulator to calculate deformation can provide multiple benefits, specially the capability of having the deformation calculated to every region of the workpiece.

Finally, the comparison of the workpiece deformation calculated by the simulation and the real data showed a similar pattern regarding the deformation over time during the experiment, but with some errors. It was possible to realize the sensibility of the used methodology and its many possible sources of errors, with a highlight for the interpolation procedure and the used coefficient of thermal expansion. The simulation returned an average error of 28.35% over the real measurements and 8.73% over the linear temperature expansion theoretical value.

In the next section is an overview of the document organization by chapters.

1.1 DOCUMENT ORGANIZATION

This document is divided into five chapters to further explain the applied technologies, their necessity, and the development of this work. The chapter 2 presents the theoretical background of the concepts and techniques used in this work, the used technology, how they function, and important concepts to better understand this project development. The parameters of the main used equipment are also explicit in this chapter.

The chapter 3 explains the challenges faced in this project, the problems in the context of this area of study, the goals of the project, as well as the proposed solution.

All the necessary steps and procedures used in the implementation of the proposed solution are explained in depth in chapter 4. The obtained results are analyzed in detail and possible sources of workpiece deformation prediction errors are discussed.

Finally, chapter 5 presents the concluding remarks along with suggestions of topics for future works.

2 THEORETICAL BACKGROUND

This chapter brings information from multiples topics that are necessary for a better understanding of the project. It contains technical information and a background knowledge explanation about the used technologies.

Section 2.1 has technical information about the used workpiece. Section 2.2 explains what is large scale metrology and presents a tool used in many measurements. Information about the physics behind thermal expansion such as the heat transfer laws, material heat capacity, and linear thermal expansion is explained in Section 2.3. Section 2.4 brings information about thermal cameras and how they work to create an image. How a 3D object can be represented in a virtual environment is explained in Section 2.5. Section 2.6 brings the different between 2D and 3D images and possible ways to transform a 2D image into a 3D one. Section 2.7 presents a software that can use a 2D image with a 3D object to transfer temperature data. It also explains the necessary features such as Texture and UV mapping. Section 2.8 explains what is interpolation and for what it can be used, as well as the tools to perform an interpolation. The concept of Digital Twin is presented in Section 2.9. Lastly, Section 2.10 brings what is the Finite Element Method and its use advantages in engineering.

2.1 TURBINE HOUSING

As the main goal of this project is to study and investigate the thermoelastic behavior of large workpieces, a turbine housing is the chosen object of study since it is considered a large scale workpiece, it is challenging because its dimension is not uniform and it was available in the institute. For this project, just half of the real housing is used for tests, which is depicted in Figure 1. The reason for such a piece is its large size, which can suffer physical transformation depending on the temperature oscillation from industrial field environments.

The turbine housing used in this work is made of cast iron and weighs 1500 kg. The specificity of its material is presented in Table 1. In a real application in industrial environments, it surrounds a gas turbine, which can be seen in the Figure 2. Similar to what we have in the WZL institute, the image shows a red turbine housing that is being placed around a turbine. In this case, the red turbine housing is bigger than the black one used in this project. Its size can be compared to the size of the two persons next to it.

The workpiece used in this project has 9 heat pads attached to its internal structure which are presented in Figure 3, with 200 W of power each, to be activated according to tests necessity. The heat pads are controlled by a microcontroller called ESP32 that is connected to the Arduino Integrated Development Environment (Integrated Development Environment (IDE)), which simplifies the process of sending signals to the

Figure 1 – Turbine housing

Source: Personal file.

Table 1 – Physical characteristics of the turbine housing material.

Density	**Young's Modulus**	**Poisson Ratio**	**Thermal Conductivity**	**Expansion Coefficient**	**Specific Heat**
$7700 kg/m^3$	$210 GPa$	0.29	$42.6 W/m/K$	$11.1 mm/mm/K$	$470 J/kg/K$

Source: Author.

Figure 2 – Gas turbine with housing

Source: Data Center Dynamics.

operating device. In an environment with heat exchange that keeps temperature fluctuations in a moderate amplitude, such as the WZL shop floor, the process of heating the turbine housing with the heat pads can take hours to complete.

The external temperature sensor was developed by the WZL institute. It is

Figure 3 – Real picture of the turbine housing inside

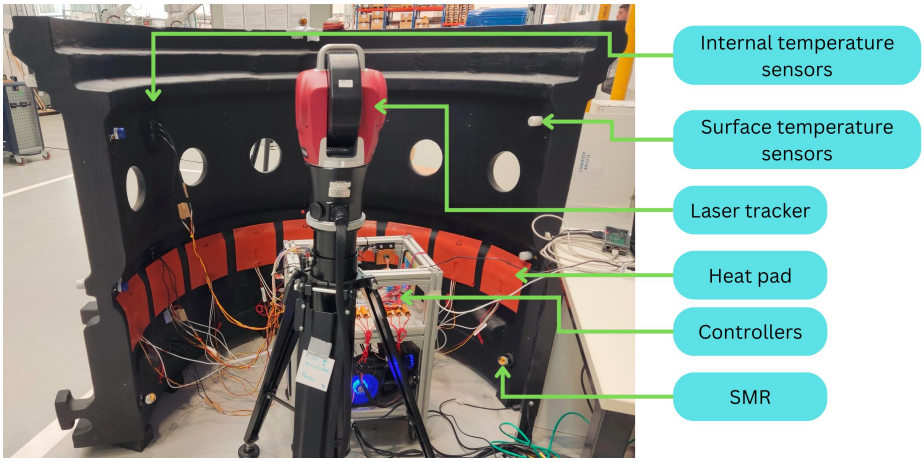

Source: Author.

connected to a database through Bluetooth and transmits its data every 3 minutes. Supporting a temperature range of 0℃ – 80℃, the sensor presents a tolerance of $0.1 + 0.0017 \times t$, where t is the temperature in Celsius. Due to its magnetic base, its handling is simple. By attaching it to the turbine housing surface and adding the sensor IP address to the microcontroller responsible for allowing the connection with the database, the temperature measurements are automatically sent to the database.

Since the workpiece is made of dense material and has thick walls, it can present a non-homogeneous temperature. This difference can happen while comparing a point on the surface and the inner region of the object. For this reason, a DS18B20 sensor was used to measure the internal temperature of some points from the turbine. It measurement range goes from -55℃ to +125℃, with $\pm 0.5C$ accuracy from -10℃ to +85℃ (DS18B20:..., 2019). In total, 9 sensors were used, divided into groups of 3. Their positions are presented in Figure 4, where the abbreviation "IS" stands for Internal Sensors. Their data were also transmitted to the same database as the external sensors with the assistance of an ESP32 microcontroller.

Considering that the turbine housing might expand or contract due to temperature changes, it is crucial for this project that these changes can be measured. For this, a Radian Laser Tracker was positioned in front of the object. The equipment can measure distance with an accuracy of $0.7\mu m/m$ by pointing a laser into a Spherically Mounted Retroreflector (SMR), which reflects the laser back to the equipment. Because of its construction, the SMR can provide a laser centering with error under 2.5µM. In total, 8 SMRs are spread over the internal surface of the turbine housing. The SMR is presented in Figure 5 (RADIAN..., 2022).

Figure 4 – Internal sensors positions

Source: Author.

Figure 5 – Spherically Mounted Retroreflector

Source: API Metrology.

2.2 LARGE SCALE METROLOGY

Large Scale Metrology (Large Scale Metrology (LSM)) was first defined in 1978 by M. J. Puttock (MAURICE JAMES PUTTOCK, 1978) as "metrology of large machines and structures... in which the linear dimensions range from tens to hundreds of meters". Together with the challenge of finding the right measurement equipment for a project, metrologists also have to consider small tolerance values regarding the deformation of the object. Regulated by the ISO 2768 standard, the tolerance for large workpieces is considerably small (STANDARDIZATION, 1989). Such small tolerances for large objects production can also be interpreted by the ratio of tolerance and nominal dimension that can reach 1:4000 for pieces with dimensions up to 2m. This highlights the necessity for

very precise measuring equipment in LSM.

Table 2 – Deviation tolerance for large scale workpieces.

Permissible deviations in mm for ranges in nominal lengths	**Tolerance class designation (description)** f (fine)	m (medium)	c (coarse)	v (very coarse)
0.5 up to 3	±0.05	±0.1	±0.2	-
over 3 up to 6	±0.05	±0.1	±0.3	±0.5
over 6 up to 30	±0.1	±0.2	±0.5	±1.0
over 30 up to 120	±0.15	±0.3	±0.8	±1.5
over 120 up to 400	±0.2	±0.5	±1.2	±2.5
over 400 up to 1000	±0.3	±0.8	±2.0	±4.0
over 1000 up to 2000	±0.5	±1.2	±3.0	±6.0
over 2000 up to 4000	-	±2.0	±4.0	±8.0

Source: ISO 2768.

Changes in the environment temperature can exert influence on the object's behavior for hours since specific material properties and a massive body allow the object to maintain temperature for a long time. For this reason, it is important to have measurement equipment capable of monitoring for hours and with high accuracy. An example of this scenario is the generation of electricity by gas turbines since its efficiency is strongly altered by the left space between the blade tip and housing (SCHMITT et al., 2016). This space can be altered by the quality of the pieces and their production dimensional tolerance.

2.3 THERMAL EXPANSION

Thermal expansion is the phenomenon in which the size of an object increases as its temperature increases. In most industrial cases the expansion of a part or a machine is not homogeneous, leading to manufacturing error and quality deterioration. Specific physical characteristics of a material can be used to predict its thermal expansion, but there are many things that can influence the change in dimension, like the temperature of the environment and the area of contact between the part and air. Understanding thermal expansion is important for a variety of fields, including engineering, construction, and materials science (LAPERRIÈRE; REINHART, 2014).

2.3.1 Heat transfer laws

Heat can be transferred in three ways: conduction, convection, and radiation. Conduction is the transfer of heat from a higher energy region to a lower energy region due to their interaction. In solids, it is mathematically described by Fourier's law

$$\overrightarrow{q} = -k\Delta T, \tag{1}$$

in which $\overrightarrow{q}$ is the heat flux density, k is the thermal conductivity of the material and ΔT is the local temperature gradient.

Convection is the transfer of heat in an object caused by the movement of fluids around the object. In this situation, the initial heat transfer occurs by convection between the object and the fluid, which carries the internal energy with its mass. Then, most of the transference is due to fluid movement. This mechanism can be natural, happening because of differences in the density of the fluid when in different temperatures, or forced by a relative velocity between the fluid and the object. For forced convection, the heat transfer is described by Newton's Law of Cooling:

$$q = hA(T - T_0), \tag{2}$$

in which q is the transference rate, h is the convection heat-transfer coefficient, A is the exposed surface area, T is the object temperature and T_0 is the fluid temperature.

Lastly, radiation is the transfer of heat by infrared electromagnetic waves. Unlike convection, which relies on the movement of matter to transfer heat, radiation can transfer heat through empty space, as long as there is a temperature difference between two objects. It is caused by thermal agitation of the object composing molecules. The heat goes from the hotter to the cooler object, which reflects part of the traveling energy.

A blackbody is an ideal object that does not reflect any radiation energy, absorbing it all. Its radiation energy can be calculated using Stefan-Boltzmann law as

$$q = \sigma T^4 A, \tag{3}$$

in which q is the heat transfer per unit time (W), σ is the Stefan-Boltzmann constant $5.6703 \doteq 10^8 (W/m^2K^4)$, T is the absolute temperature (K) and A is the area of the emitting body (m^2).

For a non-ideal object, the equation is modified to multiply e, the emissivity of the material, which is a value between 0 and 1:

$$q = e\sigma T^4 A. \tag{4}$$

2.3.2 Material heat capacity

Heat capacity is a measure of how much heat is required to raise the temperature of a substance by a given amount. It is calculated by dividing Q, the heat transferred to the object, by ΔT, the temperature increase:

$$C = \frac{Q}{\Delta T}. \tag{5}$$

Heat capacity is an intensive property, which means that it depends only on the properties of the material itself, and not on its amount.

2.3.3 Linear thermal expansion

Linear thermal expansion is the expansion of a material in response to an increase in temperature. When a material is heated, the energy of its atoms and molecules increases, causing them to vibrate more violently and take up more space. Not considering phase changes, results in material expansion.

This event is generally expressed as a coefficient of expansion *a*, which is the fractional change in length of a material per unit change in temperature. For isotropic materials, linear thermal expansion can be calculated as

$$\delta = \alpha L \Delta T, \tag{6}$$

in which δ is the linear deformation, α is the coefficient of linear thermal expansion of the material, L is the length of the material that has expanded, and ΔT is the temperature increase. The initial temperature is usually considered 20 ℃. It is important to highlight that the coefficient of thermal expansion (CTE) depends on the temperature value (JAMES et al., 2001).

2.4 THERMAL IMAGES

When used correctly, a temperature sensor can provide accurate measurements. In contrast, the sensor is capable to measure the temperature only from a specific small point to which the sensor is attached. There are occasions where getting data exclusive from a small point does not lead to the expected result since the information acquired is not enough and there is no possibility to use multiple sensors. For example, when temperature inhomogeneities occur and single-point measurements do not reflect a holistic temperature distribution, a possible solution would be to have the entire object temperature model, which can be acquired by using a thermal camera.

In order to get a thermal image of the temperature distribution of any object, a thermographic camera can be used. This camera detects the radiation emitted from the surface of the object. The information can be transformed to a temperature range, resulting in a thermal image of the object (TECHNI TOOL, 2022). The radiation is detected by the camera as an analog signal and then converted as a numerical signal, which is used to create a black-and-white image, where the luminosity is related to the radiation intensity (DÉROBERT et al., 2018).

In the Figure 6 a thermal picture of a half housing of a turbine is shown, in which the hottest regions of the object emit more radiation and are represented by the lighter parts of the image. The radiation emissivity information from an object can suffer negative influences from the environment where the object is placed before it is captured by the thermal camera. That is the reason for the correction model that transforms

Figure 6 – Thermography image

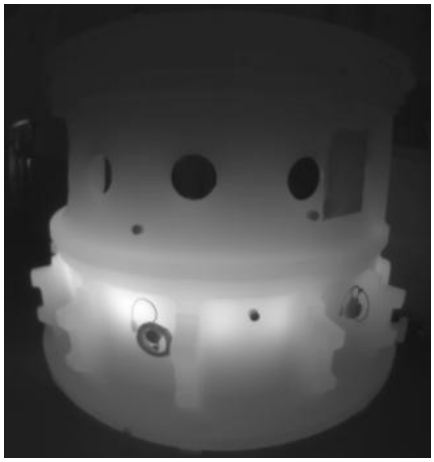

Source: Author.

emissivity into luminosity to rely on information from the object's surroundings. The total apparent luminosity received by the detector is transformed into a numerical output by

$$DL_{tot} = \tau_{atm}\varepsilon_{obj}DL_{obj} + \tau_{atm}(1-\varepsilon_{obj})DL_{env} + (1-\tau_{atm})DL_{atm} \quad (7)$$

where τ_{atm} is the atmospheric transmission for the spectral bandwidth of the camera, ε_{obj} and $(1-\varepsilon_{obj})$ are the emissivity and reflectivity of the object, respectively, and DL_{env} and DL_{atm} are the apparent luminosity from respective environment and atmosphere, respectively (DÉROBERT et al., 2018).

The camera used in this project is model IRSX-I640-F-7.5 from Automation Technology. Its specifications are presented in Table 3, where Minimum Distance of Object (M.O.D.) stands for Minimum Distance of Object. Since is a camera designed to be used in industrial environments, it has a measurement range from -40℃ to 550℃ and an accuracy of $\pm$2℃ or $\pm$2% of the measured value. [1]

Table 3 – Thermal camera specifications.

Resolution	FPS	Focal Length	Angle of View	M.O.D.	Spectral Range	Pixel Pitch
640 x 512	30	7.5 mm	89° x 69°	25 mm	7.5 to 13 µm	17 x 17 (µm)

Source: Automation Technology.

It is important to highlight that even when the camera can produce accurate images, the position where a object appears in the camera's visual field can result in a erroneous temperature reading. For a better capture of the object temperature, it

[1] Part of this section was presented in the author's mandatory internship report and is in this document to make it self-contained.

should be located at a 90° angle from the camera, both in vertical and horizontal planes (TKÁČOVÁ et al., 2010). When a object is big and close enough to cover almost the entire visual field of the camera, the most reliable information will be concentrated in the center of the object, while its edges may suffer with uncertainties.

2.5 3 DIMENSIONAL OBJECTS

The ability to create and visualize 3 dimensional (3D) object models on 2 dimensional (2D) screens is an important technological advance that has brought many possibilities to the industry. The use of 3D objects in areas such as medicine, construction, rapid industrial parts design, and engineering is becoming more evident, as numerous scientific articles are being published (BIGLINO et al., 2017), (FADERO; SHAH, 2014). (SAMPAIO et al., 2010), (WANG, J. et al., 2012).

Created from a scanner, computer-aided design software, or photogrammetry, a 3D model can be used in many computer studies, allowing physical simulations and the creation of a digital twin. For this to be possible, the structure of the object must be portrayed in the computer in a specific way called mesh. In a 3D mesh, the body of the object is divided into small polygons, usually, quadrangles or triangles, and each vertex of the geometry has its location given in coordinates. The connection between vertices generates lines, which can be combined to form a face.

Multiple software can perform the transformation of a 3D object into a mesh, with one of them being Gmsh (GEUZAINE; REMACLE, 2009). Gmsh considers that every 3D object can be created using Boundary Representation, where each representation can oscillate between four model entities, like the scheme

$$G_i^0 \Leftrightarrow G_i^1 \Leftrightarrow G_i^2 \Leftrightarrow G_i^3,$$

where G_i^0 is a vertice with dimension 0, G_i^1 is an edge with dimension 1, G_i^2 is a face with dimension 2 and, lastly, G_i^3 is a region with dimension 3. with such representation, any model can build its adjacencies of any dimension without having to process all the object.

Following this scheme, the geometry is represented differently for each model entity. A vertex is simply given by its 3D location in coordinates $\vec{x_i} = (x_i, y_i, z_i)$. An edge is its underlying curve C_i with its parametrization $\vec{p}(t) \in C_i, t \in [t1, t2]$. A face is more complex, being its underlying surface S_i with its parametrization $\vec{p} = (u, v) \in S_i$. It is important to point out that for any curve $C_j \in S_i$, any point $\vec{p}(t) \in C_j$ must be reparametrized on S_i.

2.6 IMAGE TRANSFORMATION FROM 2 DIMENSIONS TO 3 DIMENSIONS

Nowadays, most used cameras can capture 2D images, which do not have information related to the depth of the area or object contemplated. But even though a 2D image only exists in 2 axes of space, x and y, a sense of depth can be captured by the viewer just by looking at the image. This event shows that, in most cases, an image has projection information, like shadows, that are used by the human brain to establish depth characteristics at some level (KRASIL'NIKOV; KRASIL'NIKOVA, 2014). The reconstruction is only possible because the brain already has information acquired during life about our 3D world.

The use of 3D images in the industry can reach many different fields, like automotive, medicine, and robotics. Its importance is highlighted precisely because it brings more information than 2D images and allows improvements in measurement, inspection, and quality control (MOLLEDA et al., 2013). For manufacturing industries, 3D images allow the specification of position and orientation, size, identification of objects, collision avoidance, and safety. All these advantages depend heavily on suitability, accuracy, resolution, time to acquire and process data and cost (CHEOK; SAIDI, 2020), which makes it a widely researched subject in engineering.

There are many explored ways to convert an image from 2D to 3D. A couple of images that were taken at the same time but from different angles can be combined to compose a third image with depth information, creating an analogy to the functioning of the human brain that receives images from both the right and left eye (MURATA et al., 1998). Another option is the use of artificial intelligence to learn the concept of depth from multiple images, and apply the identified features to estimate the depth of new images (KONRAD; WANG, M.; ISHWAR, 2012). But both of these approaches require multiple images and some dedicated time for image processing to work.

In addition, as much as the 3D images have depth, they do not have easy connectivity with some 3D objects, which is crucial for this project. For this reason, only a 2D to 3D image transformation is not enough, and other techniques must be explored. The combination of a 2D image with a 3D object creates a visual perception of depth, even though the image does not have it. This type of integration is investigated using a software named Blender, which is explored and explained in the next section.

2.7 BLENDER

Blender is a software for 3D modeling created by Ton Roosendaal in 1994. Its main goal at the beginning was to provide a solution that allowed easy multiple changes in 3D works as they were required by clients. For this reason, Blender offers a highly configurable interface with multiple features that covers many steps of a 3D creation (BLENDER ONLINE COMMUNITY, 2018). With a great global community, blender

became an open-source software in 2002. This facilitates the process of correcting bugs and also new implementations, responding rapidly to the user's needs.

The program provides features enough to cover many areas, such as modeling, sculpting, animation and rigging, story artist, rendering, simulation, and video editing, delivering even the possibility of automation via scripting. Exploring the sculpting feature, there are numerous tools that facilitate the creation of a 3D object, like drawing, correction of shapes and symmetries, coloring, material and pattern specification, or even texturing. Although the texture tool was first designed to be a complement in object creation, it is a great feature that is explored in a different way in this project.

2.7.1 Texture

The texture is present in every single object of the world. By looking at or touching an object, we can perceive the characteristics of the object because of its texture. As an extremely common property of real life, when animations or objects are being created in a virtual environment the use of texture can enhance the designer's work and make it closer to reality (ROMANO; KUCHENBECKER, 2012).

Different methods for applying virtual textures are available nowadays. A trainable framework called Colorful Voxel Network can learn to identify the shape and color of a 2D image and create a 3D model with the same texture (SUN et al., 2018). Also, deep neural networks are being trained to recognize textures and reconstruct them in a 3D model (OECHSLE et al., 2019). Despite their great results in virtual texturing, both methods require much preprocessing of images.

In contrast, a texture method based on a UV map of 3D objects does not require any preprocessing in training, but only a 2D image (CHEN, Z.; YIN; FIDLER, 2022). Although the use of texture seeking only visual improvement of a 3D object or animation exists, its use can be further explored and bring more value than this, especially when the technique of UV mapping is applied since it relies on a 3D object mesh. This method is further explained in the next subsection.

2.7.2 UV mapping

UV mapping is a method to add virtual textures to 3D objects (BLENDER. . . , n.d.). In this technique a texture, which can be an image, is placed over a 2D plane described by (u,v) coordinates, in contrast with (x,y,z) coordinates from the object. In summary, to combine both planes a 2D planification of the 3D object mesh is calculated and placed over the texture plane. This process is called UV unwrapping and is crucial for the quality of the result (PORANNE et al., 2017).

There are multiple ways to unwrap the 3D object mesh. The most common one takes cuts from different parts of the object until it can be represented by a flat structure. It can also be explained as if the object were hollow and being "opened" up

to a stretched figure. One example of this unwrapping method is shown in Figure 7. After the unwrapping, the flat figure is placed in a 2D plane, as presented in Figure 8. Although it can result in good quality texturization, this process depends on the used texture pattern and the format of the 3D mesh.

Figure 7 – Unwrapping a cube

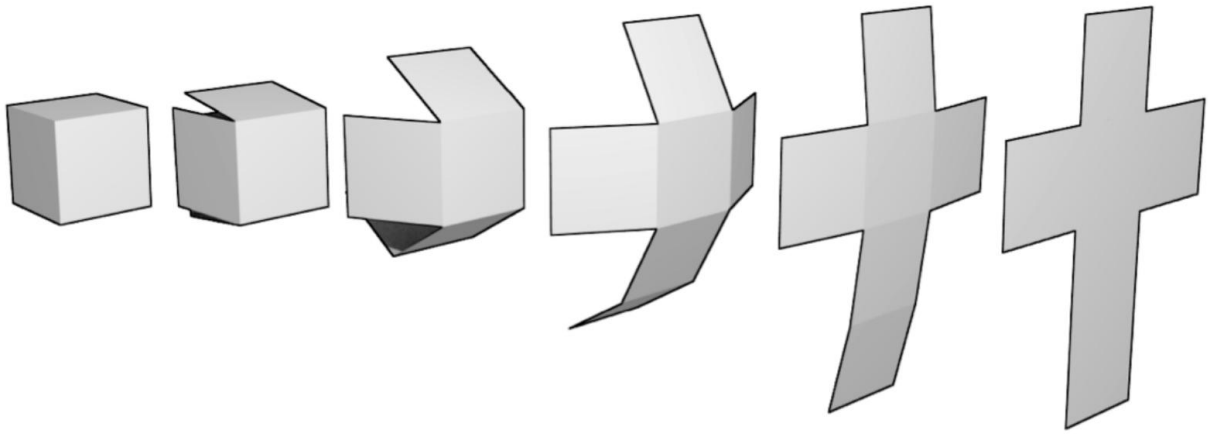

Source: (BLENDER. . . , n.d.)

Figure 8 – Cube UV map

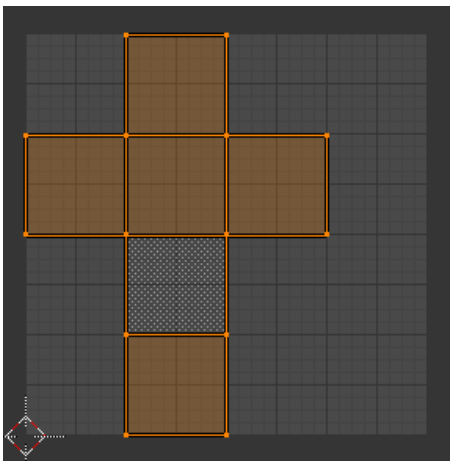

Source: RGB-LABS

The 2D UV map represents all the nodes from the meshed object in a 2D structure. This structure can be manipulated when necessary and can even change the figure format since all nodes will still be connected to a (u,v) coordinate and receive a characteristic from the texture anyhow. Since the node structure does not have to represent the object in a clear and visual manner, the whole 3D object can just be just flattened into a 2D structure. The process of flattening a 3D object and representing all

nodes into a 2D structure is called projection from view since it depends on the angle at which the object became a plane.

In Figure 9 a and b are presented two possible turbine UV maps. Letter a presents the case in which only visible nodes are placed into the UV plane, in contrast with letter b that shows how all the nodes flattened are mapped. When an image is attached to the UV plane and the UV map is projected from the view, the structure can be edited to a better fit. Figure 10 shows how the UV structure is placed after its size and shape were transformed.

Figure 9 – UV map projected from view

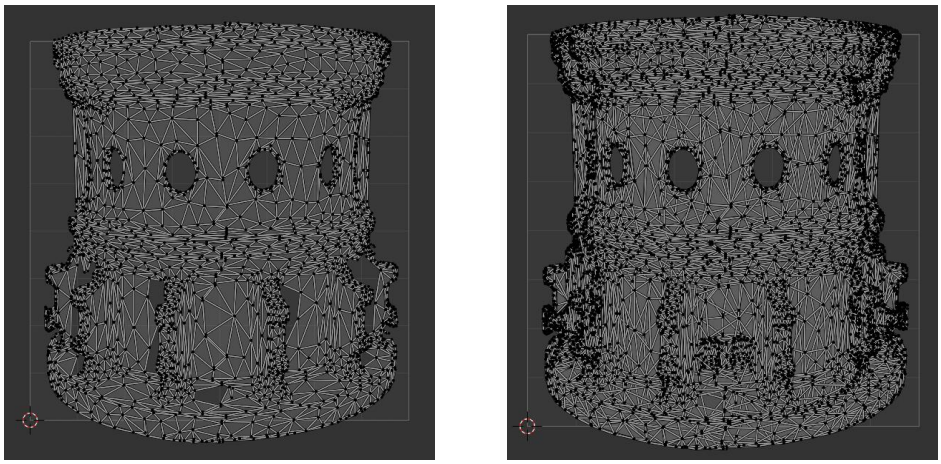

(a) Only visible nodes (b) All nodes

Source: Author.

Figure 10 – Edited UV map

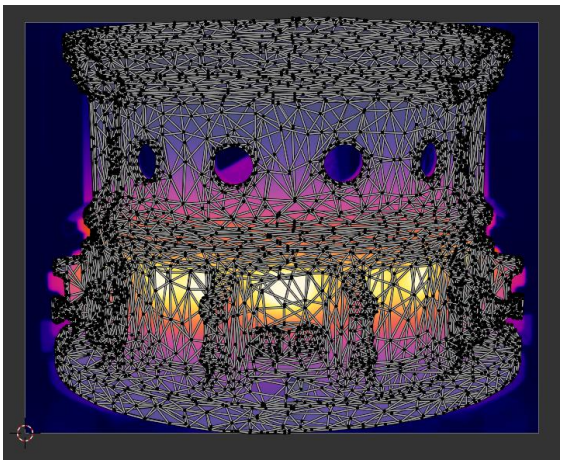

Source: Author.

By using a thermal image as a texture, the UV coordinates became a fit for the image coordinates. When the UV map from the turbine is projected into the UV plane,

every node from the object mesh is connected to a UV plane coordinate. A great benefit of using texture and UV mapping methods in this project is that with little calculation is possible to create a connection between the thermal image temperature and the node from the turbine mesh, which represents a real point from the turbine housing. To better explain all these steps and connections a diagram is presented in Figure 11.

Figure 11 – Diagram for temperature-node connection

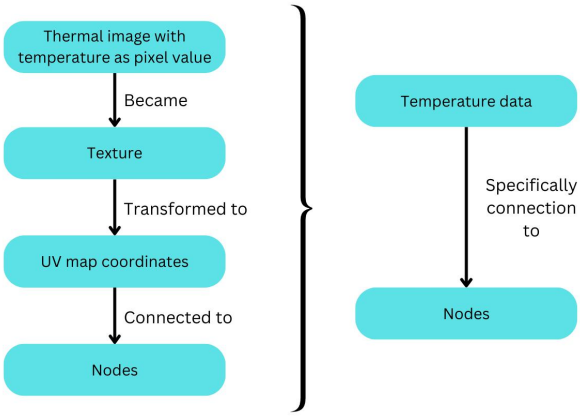

Source: Author.

2.8 INTERPOLATION

Interpolation is a mathematical estimation of new points based on already known data (STEFFENSEN, 2006). Usually, the unknown points are intermediate values of a series and can be described as a table or function (SHEPPARD, 1910). The interpolation algorithm can be used in many fields of science and engineering that require an approximation of function values, for example, temperature measurements that only acquire information from specific points instead of the whole object or place of study.

As interpolation is an estimation that can be used on several occasions, there are different methods to calculate the approximation. Each method fits better with a specific type of data and can present variations in the results, which can be more or less precise. Spatial interpolation refers to calculating a function that describes a whole surface and returns estimated values based on data that comes from a surface as discrete points or subareas (LAM, 1983). The existent spatial interpolation methods are divided into two categories: area and point interpolation.

Focusing on point interpolation, there are approximate and exact methods. The approximate methods do not conserve the already known points values, while the exact method does (CARUSO; QUARTA, 1998). One of the most used exact methods is called Kriging, created em 1960 and inspired on the work of Danie G. Krige for geostatistical

analysis in South Africa (KRIGE, 1976). There are multiple sub-types of kriging, such as universal and block kriging, but the most important one in this project is the ordinary kriging (COLUMBIA, n.d.).

2.8.1 Ordinary Kriging

The interpolation method Ordinary Kriging is based on the assumption that the variance of values is random but stationary. In other words, the mean and variance of values are constant in the space, where the variance is dependent on the distance between points (OLIVER; WEBSTER, 2015). Kriging calculates for every point the best linear unbiased estimator (BLUE) and is expressed as

$$Z_K^* = \sum_{i=1}^{n} \lambda_i Z_i, \tag{8}$$

where where Z_K^* is the estimated result, λ_i is a weight for λ_i, and λ_i is a sampled point (CHUNG et al., 2019).

An important concept used in ordinary kriging is the variogram. A variogram is a representation of the spatial continuity of a data set, which can provide information that usually is not represented in common descriptive statistics and histograms. This missing information is crucial for spatial prediction (BARNES, n.d.). The variogram is calculated by

$$\gamma(h) = \frac{1}{2N(h)} \sum_{\alpha=1}^{N(h)} [Z(x) - Z(x+h)]^2, \tag{9}$$

where x is the coordinates from position α, $Z(x)$ is the value from α, h is the distance to which an estimate is to be made, and $N(h)$ is the number of paired comparisons for h (CORREIA, 2010). The change in h returns semi-variances and these originate a sample variogram for the used data set (OLIVER; WEBSTER, 2015).

To keep the algorithm unbiased, all the used weights must sum up to 1. This means that if Z_V is a known value and Z_K^* is an estimated value, then

$$EZ_V - Z_K^* = 0, \tag{10}$$

because the increments are expected to be zero. With such constraint the estimation variance of kriging is

$$\sigma_K^2 = E(Z_V - Z_K^*)^2 = \overline{C}(V, V) + \mu - \sum_{i=1}^{n} \gamma_i \overline{C}(\upsilon_i, V), \tag{11}$$

where $\overline{C}(V, V)$ represents the covariances between sample variables, υ is Langrange parameter, and $\overline{C}(\upsilon_i, V)$ the covariances between the sample variable and the estimates (OLIVER; WEBSTER, 2015), (WACKERNAGEL, 1998), (CHUNG et al., 2019).

The ordinary kriging algorithm can return the estimated value for each point of the data set as presented in this section. But part of its calculations relies on information about the distance between every point. For this, another algorithm can be applied, such as the Dijkstra. Dijkstra's algorithm is explained in the next subsection.

2.8.2 Dijkstra's algorithm

Dijkstra's algorithm, created by Edsger Wybe Dijkstra, finds the shortest path between two nodes in a graph (DIJKSTRA, 1959). With many use cases, like robot path-planning (WANG, H.; YU; YUAN, 2011) and path optimization for vehicles evacuation (CHEN, Y.-z. et al., 2014), the algorithm can also be used to find the closest node for every other node in a 3D object, which can be useful in a subsequent interpolation.

The algorithm is considered to be node labeling and greedy, which means it is programmed to make the more optimal choice for every stage disregarding any future consequence. An important requirement for the algorithm to be applied is that there are no negative distances between nodes. The label system works with two labels: an upper limit $d(i)$ for the shortest path between the source node s to a node i, and the previous node p regarding i in the settled shortest path to i. With this information established, the algorithm can be represented in 3 steps (GASS; FU, 2013):

- Step 1: Specify $d(i)$ for every node representing the upper limit for the shortest path attempt from s to i. On the first scenario, if $d(s) = 0$, $d(i)$ is set to ∞. Then, s receives the label $\{0, –\)$, and the last node y is s.
- Step 2: For the next scenarios of unlabeled nodes, $d(i) = min\{d(i), d(y) + c_{yi}\}$, where c is the distance between a pair of nodes. In other words, the distance c_{si}, is the distance labeled on the previous node p, plus the distance between the actual and previous nodes. If the node i already has a label with a greater distance than the present one, change it to the actual value, otherwise, keep the old value. When labeled, $y = i$.
- Step 3: If all nodes have a label the algorithm has finished and the shortest path from s to any i is on the label $\{d(i), p\}$. If not, repeat step 2.

2.9 DIGITAL TWIN

A digital twin is a virtual representation of a physical object. It usually contains physical information like the main material and its properties, size, and temperature. It is typically created using data and simulations, and it is used to model the behavior and performance of the physical object or system. Digital twins are often used in manufacturing, engineering, and other fields to help improve the design, operation, and maintenance of physical systems.

The term digital twin was first used by David Gelernter in his book Mirror Worlds in 1993. But was not until 2002 that its concept was defined and brought to the industrial context by Dr. Michael Grieves (GRIEVES; VICKERS, 2017), who defined digital twin as "a set of virtual information constructs that fully describes a potential or actual physical manufactured product from the micro atomic level to the macro geometrical level".

There are many types of digital twins used in the industry nowadays, depending on the specificity of the application. A product digital twin can improve the design of new products by allowing tests and product validation in different environmental conditions. The results lead to fewer prototypes and development time while increasing quality. Production digital twins can facilitate the analysis of an actively running manufacturing process before actual production begins, reducing risks of malfunction and accidents under any possible scenario. Both product and production digital twins can be combined to create predictions for better maintenance, improvement, and efficiency (SIEMENS, n.d.).

Regardless of the type, the digital twin is created using data and simulations, and it is used to model and analyze the behavior and performance of the physical system. Its proper use can help to improve design, operation, and maintenance, and to identify ways to reduce costs, increase efficiency, and enhance customer value. It is also a great tool for science since simulations using digital twins are easily viable and can return significant information.

2.10 FINITE ELEMENT METHOD

With the advance of science, engineers have been facing challenges regarding the feasibility of complex projects. The costs of a study and the available time for research increased the need for a powerful simulation tool that could digitize physical events related to an object. The use of digital twins in the industry brought to science the digitization of objects and their physical properties but was still not enough to simulate different scenarios where temperature, pressure, weight, and other properties are quickly changed, allowing a study of the consequential natural phenomena.

In order to analyze the changes in complex physical systems, researchers describe objects' behavior through mathematical models that contain partial differential equations. By solving these equations in an automatized manner, it is possible to simulate physical events related to a change in the object scenario. With this purpose, one of the most used tools is the Finite Element Method (FEM), which requires great computer effort to transform differential equations into algebraic ones (**Dhatt.2012**). The method is based on the variations principle and triangulated or piecewise approximation, which basically says that a line or a curve can be represented by many broken pieces, where the smaller the subdivision, the closer the approximation (FENG; ZHONG-CI, 1996).

The method divides a structure into finite subdivisions of fundamental elements,

like points, lines, areas, and volume. Then, the wanted value or property can be calculated by the approximation of the sum of all elements' calculated values, since it is easier to process smaller parts. Mathematically, this process transforms a complex function with infinite degrees of freedom into a function with limited degrees of freedom. Such an approach makes the method useful for different applications while bringing an efficient and quality solution.

FEM can be applied in the civil engineering field for the structure analysis of buildings and bridges and their behavior under different conditions. Simulations using FEM in this particular area usually have a bigger focus on stresses and strains of the structures caused by great loads, seeking a better understanding of safety (KAVEH, 2014). Another possible area of study using this method is fluid dynamics. It can calculate scenarios of different pressure and velocity of the fluid as well as the efficiency of the system (CONNOR; BREBBIA, 1976). FEM can also benefit electromagnetic studies by providing information about the behavior of electromagnetic fields and currents. This way, projects related to motors, generators, and transformers can have their performance predicted to a possible improvement of efficiency (JIN, 2015). Lastly, the method is also capable of analyzing heat transfer events and their consequences. The conduction or convection of heat through solid objects and fluids can be calculated for a better understanding of the physical changes, predicting the temperature distribution (LEWIS, 1996).

The use of the Finite Element Method in studies brings advantages and disadvantages (IEEE, n.d.). As advantages it is possible to highlight:

- Ability to handle complex geometries. The method is able to accurately model these complex systems by dividing them into smaller and simpler elements that can be solved independently;
- Versatility. FEM can be applied to a wide variety of problems, from simple beam structures to complex fluid flows. This makes it a versatile tool that can be used in many different fields and applications;
- Accuracy. FEM can provide accurate solutions to complex problems. This makes problem-solving easier and more practical, besides being faster than a manual solution;
- Ease of use. The tool is relatively easy to use, especially because there are many commercial softwares that automatically perform the method without requiring advanced mathematical knowledge;
- Boundaries. By using a software, it is easy to set boundaries that specify conditions for the model to follow. It can be forces, thermal effects, and positional constraints.

At the same time, the disadvantages include:

- High computational cost. FEM requires a significant amount of computational power, especially when solving large or complex problems, which can be impractical in some situations.
- Approximate solutions. Although FEM can provide results close to reality, it is still not an exact method. It is possible to get more accurate solutions with analytical methods.

3 PROBLEM DESCRIPTION AND PROPOSED SOLUTION

This chapter presents an overview of the university and institute where this work was developed, exposing their work areas. In the sequel, the problem that instigated this project is explained, as well as the proposed solution.

3.1 THE UNIVERSITY

The Rhenish-Westphalian Technical University (RWTH), or in German “Rheinisch-Westfälische Technische Hochschule“, is, nowadays, the largest technical university in Germany. The university is considered one of the premier European educational and research institutions, covering the areas about Mathematics, Computer Science and Natural Sciences, Mechanical Engineering, Electrical Engineering and Information Technology and School of Business and Economics.

With many campuses spread in the city of Aachen and successful industry cooperation, RWTH University has a commitment to technological innovation and quality education and promotes a great incentive to research. This work was developed in one of its institutes, WZL, which is described in the sequel.

3.2 THE INSTITUTE

The Laboratory for Machine Tools and Production Engineering or, in its original German name, *"Werkzeugmaschinenlabor"*, also known as WZL, is part of the RWTH Aachen University and has a goal of making it possible to use the knowledge and results from research in the university environment. The institute allows students to work as research assistants for the employees as a learning opportunity so that he or she gains both theoretical and practical knowledge.

As a research laboratory, it has many fields of work that cover the production technology area, like business areas of development and design, quality management, organization, work preparation, production, and assembly, as well as control and automation. To allow research and work experience for the students, the institute also has an industrial field with many units of machinery used in real industrial processes.

This work was developed at the Large Scale Metrology Group, which is part of the Production Metrology and Quality Management field. The importance of this project to the institute and the problem addressed are explained next.

3.3 PROBLEM DESCRIPTION

Virtual climatization, or the use of different measurement tools and data processing to compensate changes, is an area of interest in WZL. The institute has different

projects within this area, since it is becoming an important tool in industries nowadays. In special, the virtual climatization of large workpieces is being studied, with a goal of creating a methodology to compensate the deformation caused by temperature variation in the manufacturing process, which can lead to multiple disadvantages.

Considering that the deformation of a workpiece caused by its temperature is a physical phenomenon difficult to control, since the very friction of production can raise the temperature of the part, it is necessary to have a method that compensates the deformation based on temperature ranges. However, a compensation method for this case is not trivial, since it has to happen before or during the manufacturing process, avoiding defective final products. This is because a late compensation cannot be applied, since the product would be finished, i.e. it would have no effect on the final product, only pointing out the error.

According to the International Organization for Standardization, specially the ISO 2768, the error tolerance for large workpieces decreases as the object size increases. Errors with values higher than tolerated can result in problems in the manufacture of the product and, consequently, loss of product quality and efficiency, as well as compromised product safety. In the production of large-scale workpieces, the object can change sizes according to the fluctuation of its temperature, which is influenced by the environment. Such changes can result in a thermoelastic response of the object's material, causing an expansion or contraction of the piece in the micrometer range.

With this in mind, the compensation methodology needs a technology capable of predicting the deformation of the object based on temperature ranges, considering the spatial distribution of the workpiece. This is particularly important because parts with non-trivial shapes can suffer from even greater manufacturing, complicating the calculation process for compensation.

Large manufactured parts, such as turbine housings, often do not have trivial shapes, making it difficult to understand their thermoelastic behavior. Different projections attached to the object's body facilitate heterogeneity of the object's temperature, generating different changes in the object's size depending on the region being analyzed. The impossibility of generalizing the thermoelastic behavior makes it difficult to monitor the part with measurements in the manufacturing process.

In the next section a possible solution for this problem is presented.

3.4 PROPOSED SOLUTION

In order to solve the presented problem, this work aimed to propose a methodology for acquiring data from the piece while in different temperature conditions and use it to predict the expansion suffered by the part according to the temperature change. The predictions must be based on the physical characteristics of the object. A specific goal is the development of a digital thermal twin of a turbine housing so that it can be

further exploited to enable a prediction of the workpiece expansion when heated.

All data, including temperature and deformation, necessary to the development of the proposed solution can be acquired during an experiment with the workpiece. The experiment must happen with the object under different temperature ranges, and the thermoelastic behavior of the object needs to be constantly monitored. This way, reliable data that connects temperature and deformation can be used in the future for analysis.

Since controlled temperature changes are important for the outcome of the study, the object can be purposefully heated using an external heat source. The temperature of the object should be monitored by sensors at specific points and thermal cameras for a wider coverage of the object. At the same time, a laser tracker can measure different points on the turbine and return relevant data for the deformation analysis of the workpiece.

All data acquired during the experiment must be processed. This includes the calibration of the thermal images and their transformation to a temperature unit, such as Celsius. It is worth noting that all measurement tools used must be properly calibrated. After the images have been processed, they must be used as a source of temperature data for a virtual 3D object, effectively passing 2D data to the 3D plane.

The distribution of temperature in the virtual object is extremely important. The proposed tools can only measure the temperature on the objects surface, which is not enough for this project. To solve this particularly issue, an interpolation method can be applied to extend temperature value to the inside of the object.

In order to create a reliable digital thermal twin (Digital Thermal Twin (DTT)), a 3D virtual object with the same dimensions as the original object needs to be used and the temperature distribution must respect the heating pattern observed in the real experiment, even if some regions are warmer than others. Finally, with a digital thermal representation of the object, a simulation can be performed to predict deformation based on temperature. The simulation must consider the physical properties from the object, since they can cause great influence in the results.

Simulating a physical event is not trivial and requires a lot of processing. For this reason, the DTT can be processed by a finite element method (FEM) simulator, which used the object's physical properties to calculate and predict the most likely outcome regarding the object's deformation. The simulation results can then be analyzed and compared with the real experiment data to observe how well the simulator predicts the object deformation. Also, it is important to analyze and highlight possible sources of errors in the final result.

For a successful result, many steps may be necessary during the development of the project. Tasks such as temperature sensor calibration, finding the positions of the target for the laser tracker, setting the laser tracker routine, camera calibration,

processing the thermal images, assigning the correct temperature to each node of the virtual object, and many others will be essential. In summary, the main topics of this solution are visually represented in the Figure 12.

Figure 12 – Proposed solution diagram

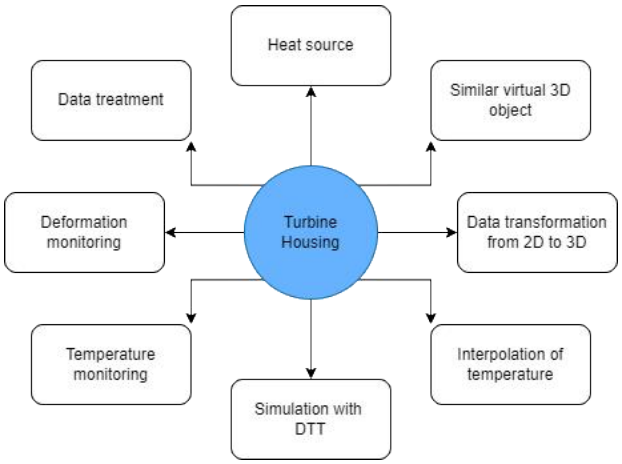

Source: Author.

The diagram brings as main topics, all related to the turbine housing, temperature and deformation monitoring, data treatment, heat source, similar virtual 3D object, data transformation from 2D to 3D, interpolation of temperature and simulation with a DTT. The implementation of the proposed solution is explained in details in chapter 4.

4 PROJECT DEVELOPMENT AND RESULTS

As a large workpiece can suffer from temperature variations resulting in thermo-elastic deformations, a methodology to predict this behavior is needed in order to have a system capable of compensating changes in the object size during the manufacturing process. As presented in chapter 3, this work used experimental data from a turbine housing in order to perform a FEM simulation of the workpiece behavior under different temperature conditions. All the necessary steps to perform the simulation, the simulation results and the comparison of simulated and real data are exposed in this chapter. To provide a better view of the following steps, an diagram is presented on Figure 13.

Figure 13 – Experiment diagram

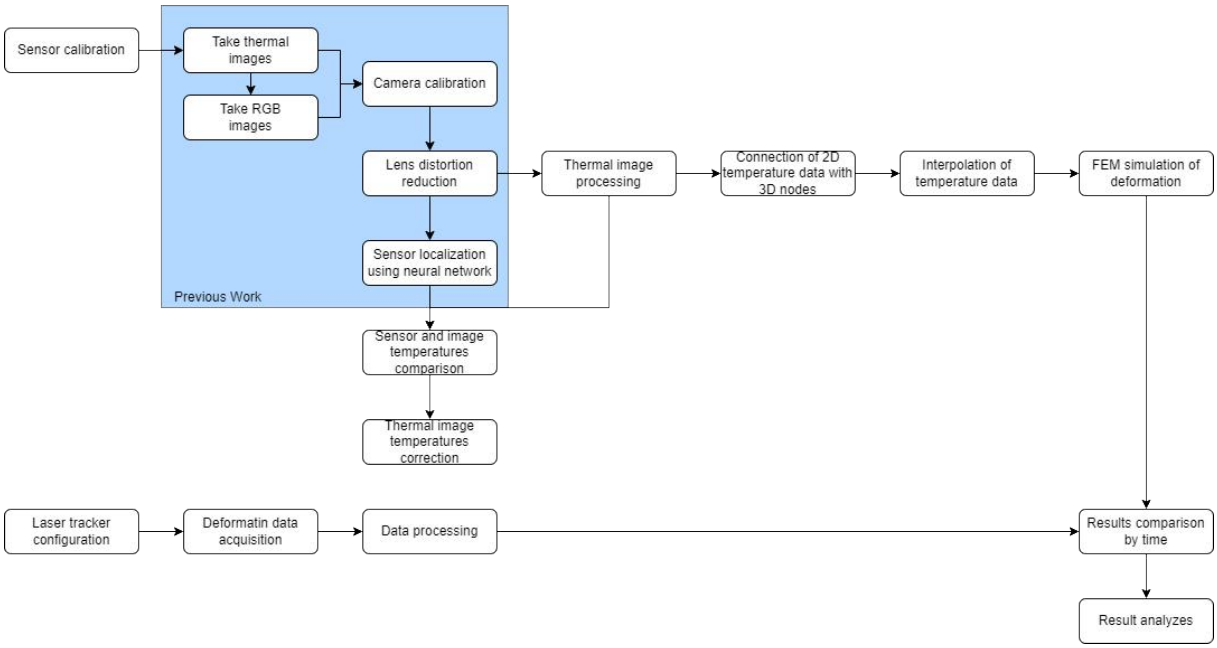

Source: Author.

Figure 13 has the main steps of this project in an ordered diagram. It also covers some important steps from previous work, which are the temperature sensors calibration and installation, RGB and thermal camera setup, image distortion treatment, and sensor localization using neural network.

Further steps developed in this work follow the order of correcting thermal images temperature, processing thermal images to transform the camera values in Celsius, connect the thermal image pixels to a 3D object in order to transfer temperature data to the virtual object, interpolate the known temperatures to improve temperature distribution through the virtual workpiece, and create the digital thermal twin in the FEM simulator. Then the final steps are retrieving and treating data from the simulation and compare the results with the real experiment data.

Considering the importance of understanding the steps developed in previous

works, the next section brings an explanation of what was developed and their necessity for this project, as it is a continuation of what has been achieved. After that, the steps of the proposed solution in this work are explained in details. Lastly, a section containing all the procedures performed in sequence for the actual experiment is presented, as well as the results analysis.

4.1 SENSOR LOCALIZATION

It is important to highlight that the first steps in the development of the global project were proposed and implemented by the present author in a previous internship, as described in the report. For this reason and for a better understanding of this work, a simplified summary of the work is presented in this section.

In order to acquire the temperature from the whole surface of the turbine housing, a thermal camera was used to capture a thermal image, which may present high measurement uncertainty. To solve this problem there is a possibility to use more precise temperature sensors to calibrate the image. The calibration procedure requires non-trivial data such as the sensors' position. This is because the thermal images have low quality, making it hard to identify the sensor through the image.

To solve the low-quality image problem, a second camera was used. This camera was a usual camera that captures RGB images with high quality. Then, images from the turbine housing with attached sensors were taken with the high-quality camera and processed by a neural network algorithm called Faster-RCNN, which was able to identify the sensors' position on the RGB image. After this, is still required to get the sensors' position on the thermal image, and for this is necessary a pixel conversion method between the images.

A pixel conversion with low error must consider the distortion present in each image since both cameras have different lenses. To reduce the distortion, an algorithm that computes the intrinsic parameters of the camera was applied. It can determine the distortion caused by the lens and reduce it on each image. After reducing the distortion in every image, the size of the images was considered as a factor to calculate the pixel conversion between thermal and RGB pictures.

4.2 PROJECT STEPS IN DETAIL

4.2.1 Sensor Calibration

To improve the accuracy of the experiment and its results all the used temperature sensors have gone through a calibration process. All sensors transmit data via Bluetooth and can also be connected to a computer to receive calibration parameters. The used algorithm, developed by previous workers, reads the temperature from the

sensor in cold and hot conditions and, with external industrial sensor data, calculates the calibration parameters.

The calibration process uses a cooler container to simulate a cold or hot homogeneous environment. The sensors are placed in a container filled with water, but not fully submerged. Then, an industrial temperature sensor is placed on the water to measure the true temperature. The industrial sensor used is LR-Cal LRT 1000 and presents a measurement accuracy of 0.005K at 0℃ and 0.02K in the range -40...+20℃.

First, the water temperature is cold, around 23℃, and the measurements from all sensors are saved. Then, the water is heated to 45℃ and the measurements are saved again. With the information from the industrial sensor, the calibration file is calculated and sent to the sensor, increasing its measurement accuracy. An example of measurement is shown at Table 4.

Table 4 – Sensor calibration measurement values.

Sensor	**Before**	**Cold water**		**Hot water**		**After**
		Sensor	**Reference**	**Sensor**	**Reference**	
a	21.92	18.29	21.9	43.41	42.5	25.48
b	21.47	17.72	21.9	41.2	42.5	25.25
c	14308.79	-4927.93	21.9	1.34	42.5	44.36

Source: Author.

As presented in Table 4 sensors a and b had a small difference of 0.45℃ between them, while sensor c presented an extremely high number, which did not fit reality. After the calibration procedure sensors a and b had their difference reduced to 0.23℃. Sensor c had a closer number to reality than before, but still not real, so it was reported as defective and not utilized again in this project.

4.2.2 Thermal image processing

In order to be able to use the thermal images as a visual representation of temperature, it is necessary to process all images. This is mandatory since the camera saves the images by giving its own signal value range, captured by the sensors, to the pixels, which is not the temperature as we know. The signal value is directly related to physical properties from the camera, the object and the environment, which allows a calculation to transform the camera signal value to Celsius. All the thermal images used were saved in .npy format, in which the image is represented my a multi-dimensional vector and every pixel has a space, allowing a specific and separated transformation. A schematic of temperature measurement by the camera is presented in Figure 14.

The figure shows the dependence that the signal has, not only on the object but also on the atmosphere and the lens. It also presents the used symbols and parameters, such as:

Figure 14 – Emission and transmission parameters of a real measurement situation.

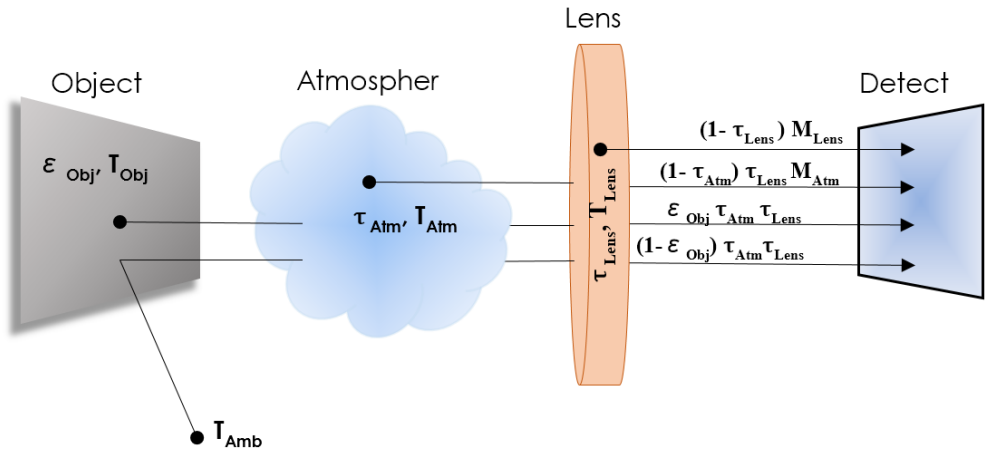

Source: IRSX User Manual.

- $_{Amb}$ = Ambient Temperature
- ε_{Obj} = Emissivity of the object
- T_{Obj} = Temperature of the object
- τ_{Atm} = Transmission of the atmosphere
- T_{Atm} = Temperature of the atmosphere
- τ_{Lens} = Transmission of the lens
- T_{Lens} = Temperature of the lens
- S_{Det} = Detector signal in counts
- $M(...)$ = Radiation (temperature-dependent)
- τ_{Lens} = Transmission of the lens

Since the images have temperature data in the signal unit, a conversion to Celsius or Kelvin is important. This procedure was performed with a *Python* script that reads each image, converts the signal to Kelvin, and saves all the new values as a new image. The necessary equations were taken from the IRSX manual (AUTOMATION TECHNOLOGY, n.d.).

First, considering that the experiment was performed in a air conditioned environment, the variables for the temperature of the environment, atmosphere, and lens were set at 295.15K. Since the camera and the object were a short distance away, the transmission of the atmosphere was set to 1.

$$\varepsilon_{\tau} = \varepsilon_{Obj}.\tau_{Atm}\,, \tag{12}$$

and the emissivity of the object considering the atmosphere and the lens

$$\varepsilon_{\tau 2} = \varepsilon_{Obj}.\tau_{Lens}.\tau_{Atm}\,, \tag{13}$$

were calculated.

Then, the radiation of the environment (I_{Amb}), of the atmosphere (I_{Atm}) and of the protective window (S_{Atm}) of the lens were calculated using the radiation equation

$$I_{Atm} = \frac{R}{e^{\frac{B}{T_{Atm}}} - F}\,, \tag{14}$$

$$I_{Amb} = \frac{R}{e^{\frac{B}{T_{Amb}}} - F}\,, \tag{15}$$

$$S_{Atm} = \frac{R}{e^{\frac{B}{T_{Lens}}} - F}\,, \tag{16}$$

where R, B, and F are based on the physical Planck function and given by the thermal camera manual (AUTOMATION TECHNOLOGY, n.d.). Also, the radiation components K_1 and K_2 were calculated as

$$K_1 = \frac{1}{\varepsilon_{\tau 2}}\,, \tag{17}$$

and

$$K_2 = \frac{1-\varepsilon_{Obj}}{\varepsilon_{Obj}}.I_{Amb} + \frac{1-\tau_{Atm}}{\varepsilon_{\tau}}.I_{Atm} + \frac{1-\tau_{Lens}}{\varepsilon_{\tau}}.S_{Atm}\,. \tag{18}$$

Then, the object signal (S_{Obj}) is calculated as

$$S_{Obj} = K_1.(S-O) - K_2\,, \tag{19}$$

where O describes the signal offset (property of the detector). Finally, the temperature of the object (T_{Obj}) can be calculated as

$$T_{Obj} = \frac{B}{log\left(\frac{R}{S_{Obj}} + F\right)}\,. \tag{20}$$

After performing the conversion from camera signal to Celsius for every pixel in all images, the images now have readable temperature data and can be used in further steps. Next section explains how the 2D thermal image can be used as information for a 3D object, connecting pixels to 3D nodes.

4.2.3 Connection of temperature data with 3D nodes

After acquiring images from the turbine housing with good-quality temperature data, the next important step in the development of this project is to combine the images with the real object. The goal of this task is to transform the 2D image into a 3D image that respects the format and size of the object.

With this goal, a computed 3D model of the turbine housing was used. This model was imported to a software named *Blender*, which allows different types of manipulation on 3D objects, including its texturing. By applying an image to the object surface as a texture, each node of the 3D object is connected with a pixel from the image. Using the pixel data, it is possible to calculate the corresponding temperature, which is explained later. Thus, simply put, the thermal image applied to the 3D object makes the temperature become the texture of the turbine housing.

The texture feature uses a UV mapping of the 3D object, which can be positioned on a chosen image for better fitting. The UV map comes from the node structure that forms the object. This structure is presented on Figure 15, where is possible to see all the nodes and their connections from the turbine housing.

Figure 15 – Turbine housing structure.

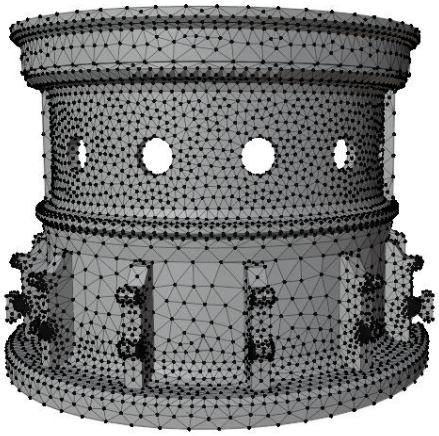

Source: Author.

At first, the UV map used was from the front view of the object, transforming the 3D structure into a flat structure that still represents all the nodes from the object. Then, the UV map was placed over one thermal image. Both image and UV map fitting are presented in Figure 16 a and b.

Even with an apparently good fit, the result of the procedure was not successful. This is because *Blender* has an internal automatic interpolation to fill the areas that are not contemplated on the view. For example, the sides of the lower small parts are not visible if the turbine housing is positioned with a front view. This makes the software

Figure 16 – UV mapping fitting with one image

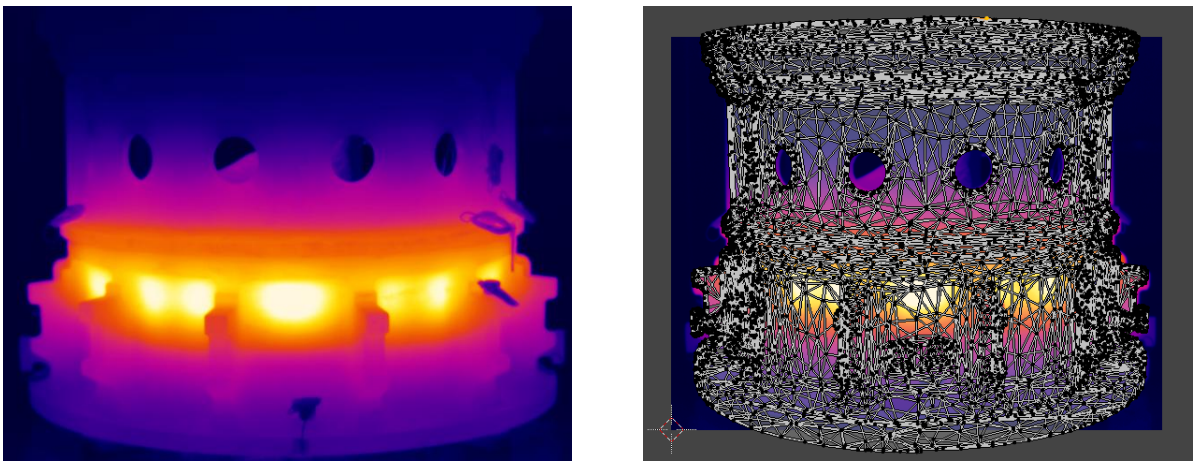

(a) Thermal image (b) UV map

Source: Author.

extend the data from some points to the closest point that is not covered yet. The result of this fitting, along with the explained problem, are presented in Figure 17. The lateral view on Figure 17b shows unwanted patterns on the object texture, which leads to erroneous temperatures.

Figure 17 – UV mapping result with one image

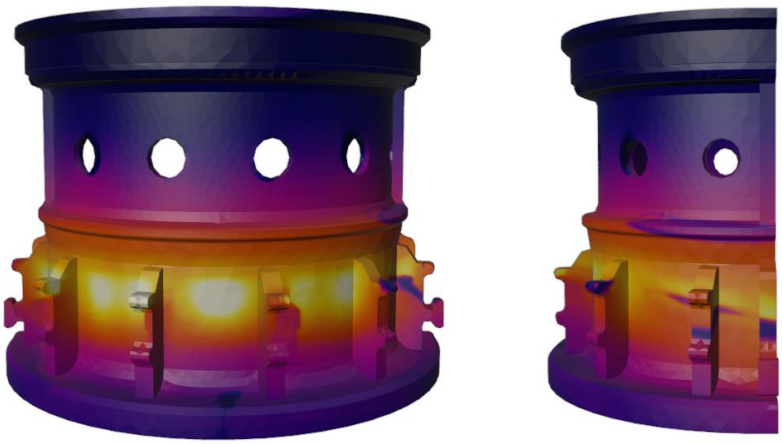

(a) Front view (b) Side view

Source: Author.

To solve this problem the turbine was divided into 6 parts and the UV mapping procedure was performed separately for each one of them. For this, 6 images were taken, where each one had a different part of the turbine centered. Since the UV map for a single part was generated with a similar viewing angle of its respective image, the results showed no noticeable image distortions for the parts not visible at a given angle. For example, the same angle of the turbine presented in Figure 17b is now visible in

Figure 18 after the UV mapping for 6 parts.

Figure 18 – UV mapping result with 6 images

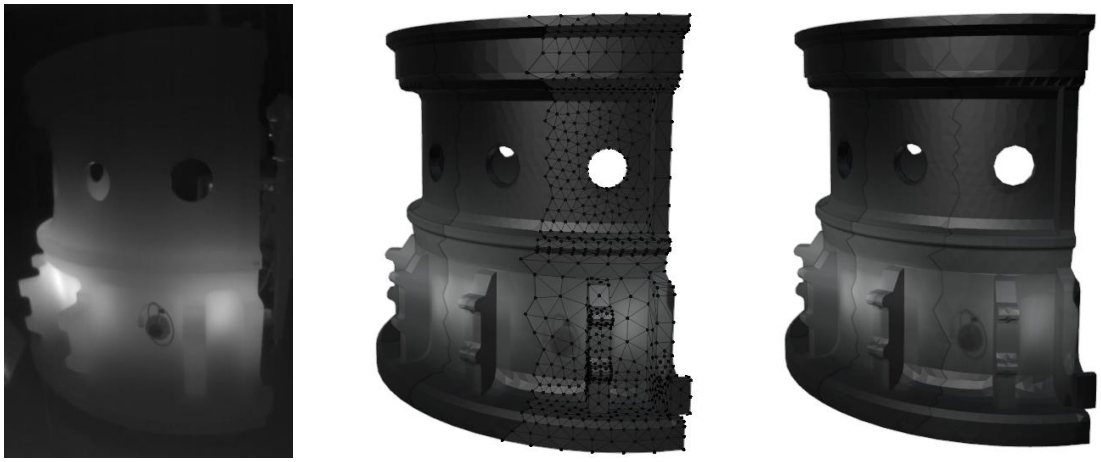

(a) Image used for the right part

(b) UV map from the right part

(c) Result from the right part

Source: Author.

Now, with every pixel of the image representing a temperature, and the 2D images attached to the 3D virtual object, the connection can be exported as a .ply file containing nodes coordinates and its corresponding pixel. It is important to remember that the .ply files does not have the temperature data itself, but the corresponding pixel coordinates in percentage from the image size. For this reason, another script was written in which all the point cloud information present in the .ply files from each division of the turbine housing 3D model was read and processed.

First, the script reads the pixel coordinates in image percentages related to each node. Then, the percentages are transformed into a pixel coordinate directly related to the 2D image plan. The new coordinates can be used to to find the pixel position in the image and its value (temperature in Celsius). Finally, the temperature value retrieved from the pixel is connected to its corresponding 3D node and this information saved in a python list. After all the nodes from the 6 parts of the turbine housing were processed, all data was saved as a .csv file.

The original 3D model of the turbine housing was created using a software named *Solid Works*. When the file was imported to *Blender*, a software that has different uses than *Solid Works*, the 3D object did not have the internal structure anymore, in other words, the object became hollow. For this reason, the procedure to connect an image to nodes only worked for the nodes from the surface of the object. But to be able to do further analysis, it is important to get a temperature value for the internal nodes. For this reason, the solid 3D object was used to perform an interpolation, which is better explained in the next section.

4.2.4 Interpolation

At first, all the nodes received a temperature value from the thermal image, since all nodes were selected when the .ply file was created. Even though the thermal data is 2D and only from a front view of the object when all nodes are selected, *Blender* transforms the front and back nodes from the object into a flat structure, so when the UV map is placed over an image the back nodes also receive information from the image.

All surface nodes had a temperature value, but the internal ones did not. To solve this, Dijkstra's algorithm was used. As a strong interpolation method, it uses the closest nodes' information to calculate a temperature value from an internal node. The adaptation of Dijkstra's algorithm to 3D objects was done by another member of the project in which this research was developed. It uses a VTK and STL file from the 3D turbine housing object to get and spread information from and through all nodes.

Using all the nodes from the surface of the 3D object the result of the interpolation was not good. The temperature value is demonstrated as different colors for different values in the image. As presented in Figure 19, the back of the turbine got random temperature values. Also, the front had some mistaken values on the lower parts of the turbine housing.

Figure 19 – Interpolation with all nodes

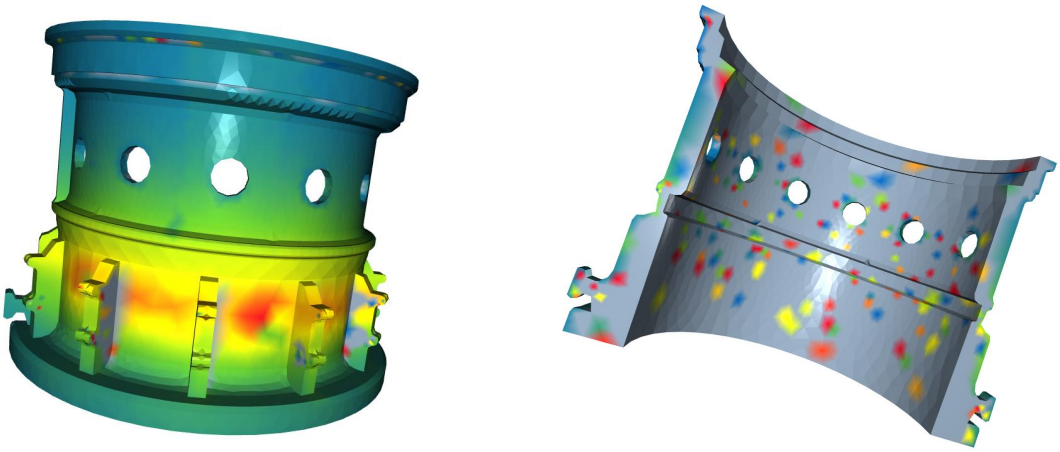

(a) Front (b) Back

Source: Author.

To investigate why this happened, an interpolation with only 24 nodes was performed. For each one of the 6 parts of the turbine housing, 4 points were manually selected on specific positions such as the front and back upper part and the front and back lower part of the object. The Figure 20 shows the result of the experiment. The algorithm returns a better result than before, but the lower parts of the turbine still do not have a good representation of the heated parts.

Figure 20 – Interpolation with 24 nodes

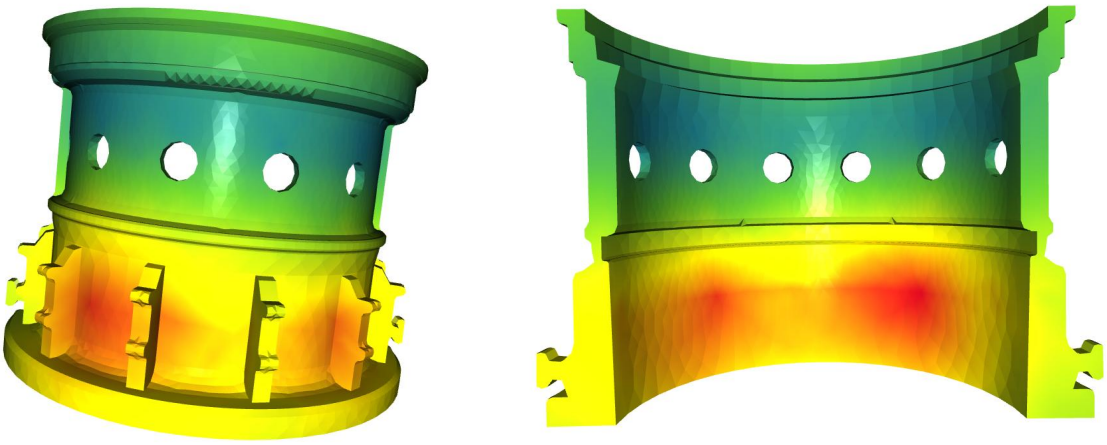

(a) Front (b) Back

Source: Author.

Tests were performed increasing the number of used nodes. With 1000 nodes the interpolation was returning random values, but with 600 it returned a better result, as shown in Figure 21. The known heated areas were better represented, but still not good enough. This is because the lower prominent parts of the object have more nodes than the rest of the lower surface and, because of the random selection of the nodes, more nodes were coming from them than the surface where the heat is greater. The position of the selected points is presented at Figure 22. The color of the nodes represent different temperature values, with red being the warmest node and blue the coldest. The gray big nodes are the selected ones.

Figure 21 – Interpolation with 600 nodes

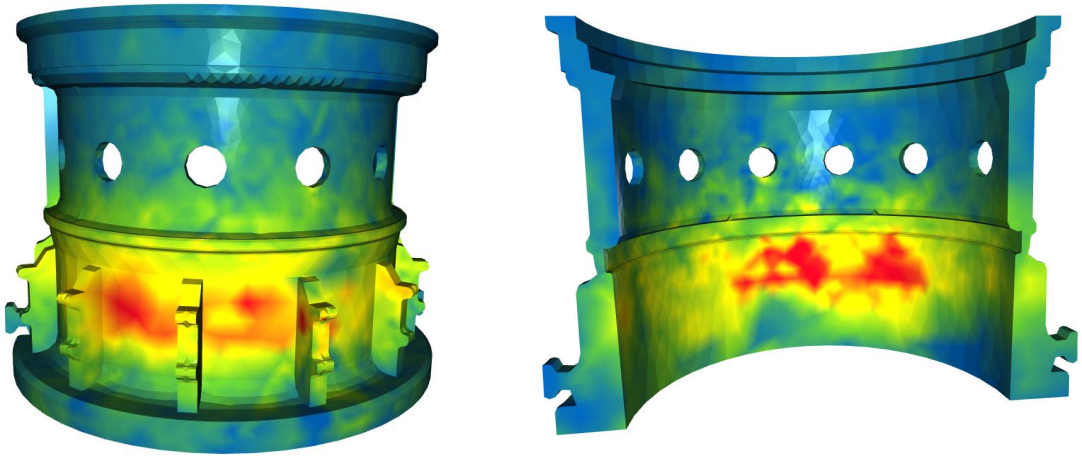

(a) Front (b) Back

Source: Author.

To solve the problem of concentrating nodes in the prominent parts of the object

Figure 22 – Points of 600 nodes

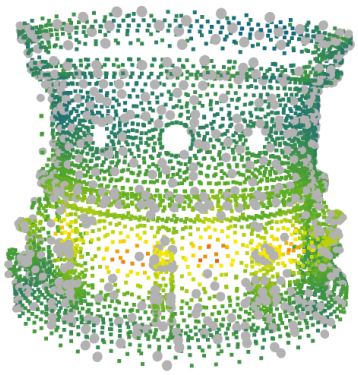

Source: Author.

and considering that the thermal image only provides information from the front surface of the turbine, nodes from specific positions were manually selected. The regions where heat is located in the front were specially contemplated in this process. 430 nodes were selected from the different regions, plus 12 nodes from the back of the turbine and more random nodes. In total, 585 nodes were used. With this approach, the selected nodes were in a more useful position, as shown in Figure 23. The result of the interpolation using these nodes is presented in Figure 24.

Figure 23 – Points of 585 nodes

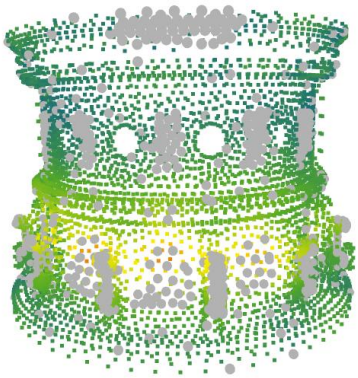

Source: Author.

It is possible to notice in Figure 24 that the heat is present with a better contour and position. It respects the real case where the hottest temperature is not on the prominent parts of the turbine, but in its rounded lower surface. This result is important for the next step since it influences all of the next outcomes.

4.2.5 Finite Element Method Simulation

To simulate a heating and cooling process of the whole turbine housing a software named FreeCAD was used. This software calculates the thermo-elastic transformation using the finite element method, which allows a more realistic simulation

Figure 24 – Interpolation with 585 nodes

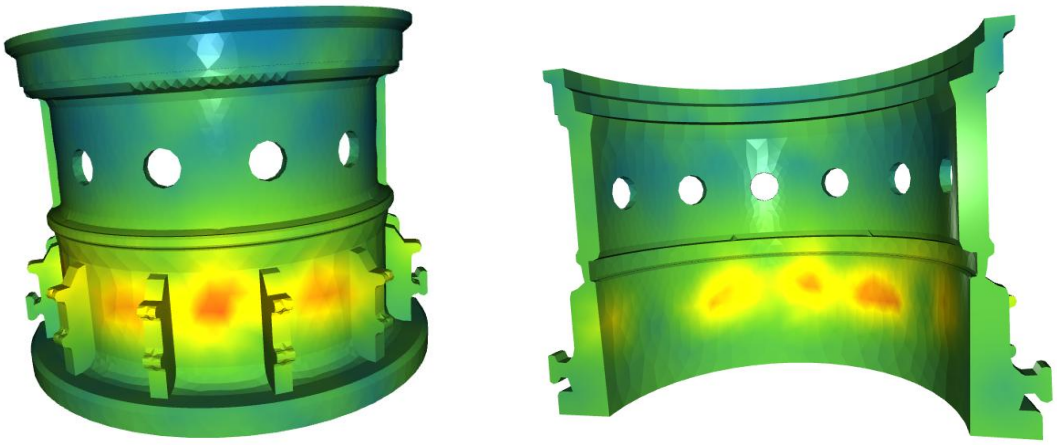

(a) Front (b) Back

Source: Author.

of the turbine housing behavior. FreeCAD has many features that allow an easy pre-configuration of the object and its characteristics, but a lot more can be done if the simulation file is configured manually and not only through the features.

The software requires the physical characteristics of the object and its material, specific constraints, and temperature data as input. The physical characteristics, presented in Table 1, and constraints were selected through software features, but the temperature data had to be manually configured since each node had a different temperature value.

Figure 25 – Mechanical boundary condition

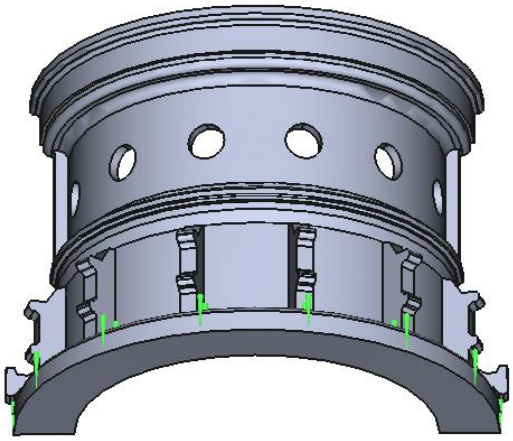

Source: Author.

One physical limitation of the object is that the bottom surface touches the ground and can not expand downwards. This specificity was added to the software as presented in Figure 25. It shows the faces of the 3D turbine housing with green arrows around the

bottom face, which represent the limitation of expansion. The temperature configuration was less straightforward and is explained in the next subsection.

4.2.5.1 Extraction of temperature

After the camera signal was converted to a temperature value in Celsius, it is important to write the temperature from each node in the order that the software FreeCAD uses. This procedure was performed at the same time as the configuration file for the simulation was edited. This file has a list of all nodes with their respective number and coordinates. This is important to know the order in that FreeCAD software works with the nodes.

Since the nodes' temperatures need to be written in the same node order that FreeCAD uses, a python script was created to edit the configuration file automatically. It reads a temperature file with only coordinates and temperature data, crosses the coordinates with the ones from the configuration file, and formulates a list with the number of nodes and their respective temperature only for the coordinates that where match in the correct order. This list is passed to a specific position in the configuration file and, then, the edited file is imported to FreeCAD.

4.2.5.2 Calculation of deformation using external temperature data

While the real turbine housing is heated using 9 heat pads that are spread on its internal surface, the simulation can not truly reproduce this event. The heating options from the software do not allow such heat configuration, and any other heat source would result in a different outcome regarding the concentration and distribution of heat in the object.

In order to simulate the heating process of the turbine, instead of adding any heat source to the simulator, external temperature data is imported to the simulation configuration file. But at the same time that the temperature is important, is also crucial that the deformation data is considered.

For this reason, temperature from a specific time of interest can be added to the simulator, while the deformation caused by it is calculated by the software. To perform this calculation, the temperature was passed to the simulator using the same procedure presented in Section 4.2.5.1. Then, the configuration file had to be manipulated again in order to implement a static simulation, instead of the usual dynamic one.

With the correct temperature information, as well with its respective deformation, the simulation was finished and its data can be exported for further analysis.

4.3 PREVIOUS EXPERIMENTAL SETUP BASED ON ROBOTIC ARM

Before the start of the project presented in this document, an experiment was conducted in which the turbine housing was heated by using the heat pads and cooled by the ambient temperature. The whole process lasted about 6 hours, of which 3 were for heating and 3 for cooling. During the whole process, the turbine temperature was measured by 25 sensors. Furthermore, the deformation of the workpiece was also measured by means of a robotic arm that was attached to the turbine. All the data was stored and available for future analysis.

In order to test the correspondence between thermoelastic simulation results and reality, 5 timesteps were selected from the experiment data. The first time corresponds to the beginning of experiment (B), the second to the middle of the heating process (H1), the third to the heating apex (H2), the fourth to the first half of the cooling process (C1) and, lastly, the fifth to the second half of the cooling process (C2). Only the temperature and deformation data from these time points were used in the analysis. It is important to clarify that all the following procedures were repeated at each time point separately.

As stated before, the real data temperature came from 25 sensors, which can only represent 25 nodes out of 6216 from the virtual turbine housing. For this reason, the rest of the nodes had their temperature calculated using interpolation. After the temperatures were calculated, the simulation process started.

The real deformation data was acquired by measuring 3 points' positions and calculating the distance between them with the Euclidian norm. The points are presented in Figure 26. Point A is considered to be the origin and points B and C are used for calculating the horizontal and vertical deformation, respectively.

Figure 26 – Old deformation measurements positions

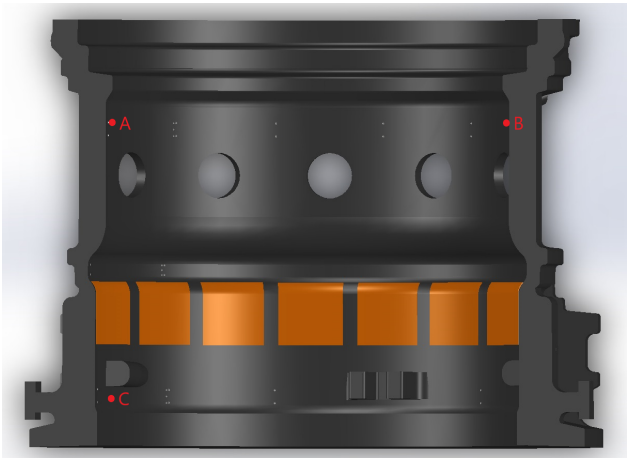

Source: Author.

The simulation data is a result of a static thermoelastic simulation using FreeCAD. The temperature was imported to the software that estimated the deformation for every

node. Then, the simulation was exported as a VTK format file, which contained all necessary data. To read this file and extract information related to the measurement points, a python script was created.

Figure 27 presents the difference between the simulation and real deformation regarding the vertical measurement, between points A and B. It is possible to notice that the values have a large gap, especially for the third point, when the heat was high. In Figure 28 the horizontal deformation, between points A and C, is shown. Although the gap between real and simulation data is smaller for the horizontal than the vertical comparison, it still exists.

Figure 27 – Vertical Deformation

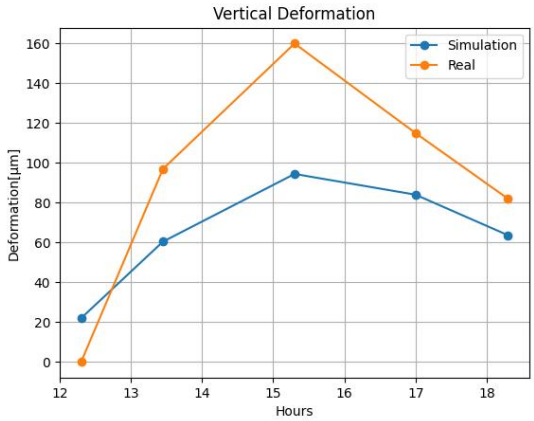

Source: Author.

Figure 28 – Horizontal Deformation

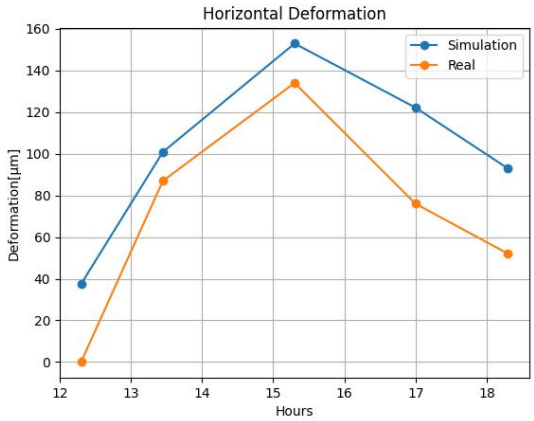

Source: Author.

The explanation for such a gap is not certain, but a few circumstances can be highlighted. First, as the robotic arm that made the measurements was attached to the turbine housing, it may have suffered a displacement during the deformation of the workpiece itself.

4.4 NEW EXPERIMENT SETUP USING LASER MEASUREMENT TOOL

After developing and testing all the presented techniques and methodology necessary, a new experiment was performed. In this experiment, the turbine housing was forced heated using 9 heat pads for 3h. Then, the heat pads were turned off and the turbine housing was left to cool down naturally. During this whole procedure, there was a thermal camera set to take pictures of the workpiece every 5 minutes, sensors monitoring its temperature, and a laser tracker measuring some specific points distances. All the procedures performed will be better explained next.

Before the actual experiment was started, the sensor calibration was already performed, as explained in Section 4.2.1. Then, continuing with preparation, the temperature sensors, and spherically mounted retro-reflectors (SMRs) had to be positioned. In total, 13 temperature sensors were attached through the inside and outside surfaces of the turbine housing, while 7 SMRs covered the inside of the object. Their positions are presented in Figure 29. All measurement points were chosen seeking the best representation of the overall characteristics of the object, which will be important for future calculations and analyzes.

Figure 29 – Measurement points

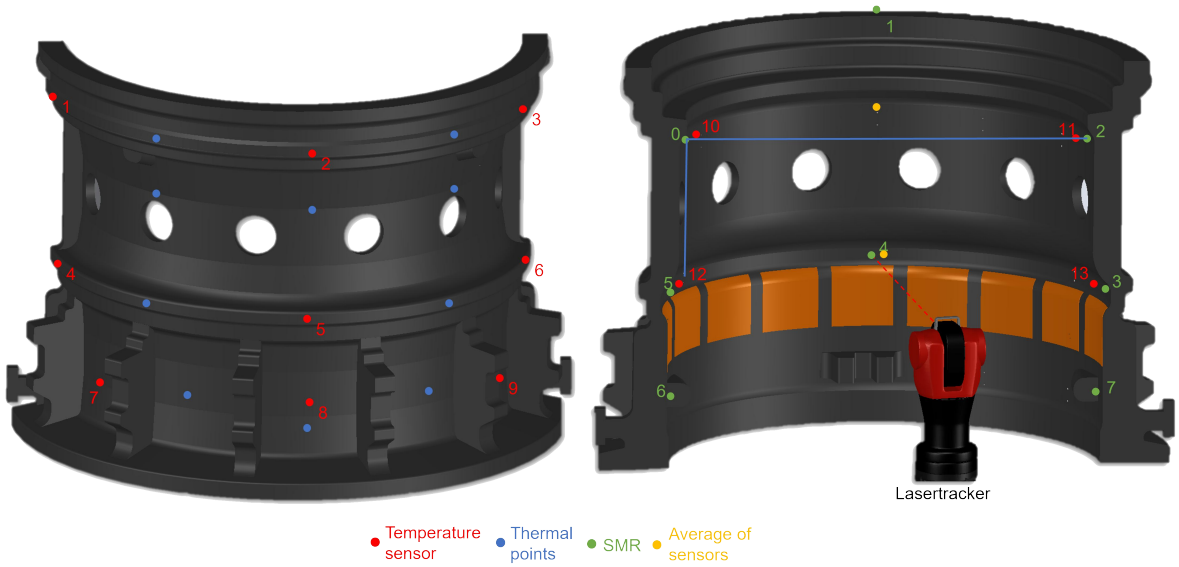

Source: Author.

In Figure 29, along with temperature sensors and SMRs, there are also yellow points that represent the average temperature of the closest sensors horizontally. Yellow point 1 is the average of temperatures from sensors 10 and 11, while yellow point 2 represents the average of temperatures from sensors 12 and 13. Besides, the blue points represent all the thermal points extracted from the thermal images. Both average

and thermal points will have their use and importance better explained throughout this section.

All SMRs received and mirrored a laser from the laser tracker device, which could measure the distance from the equipment to the target. All data was sent to a database in the format of 3D coordinates and time. The laser tracker performed a measurement routine from SMR 1 to 8 in ascending order repeatedly, in an infinite loop. Since the laser tracker is able to provide measurements with an accuracy of $0.7\mu m/m$, it allows future calculations of material expansion using the acquired distances.

For the laser tracker to work properly, it needs to be previously configured. In this step, the laser is manually pointed to every SMR and their coordinates are transmitted to the database. Also, to make the equipment perform the correct routine, a script is sent to its system, allowing it to read every SMR position in the wanted order.

After the laser tracker is set up properly, the thermal and RGB cameras needed to be positioned. For this, a tripod was placed in front of the turbine housing, targeting the center of the outside surface. The setup of the camera was chosen to get the most surface area possible with both cameras. The actual position is presented in Figure 30. Fixed on the tripod is a 3D model holder, displayed in Figure 31, that allows both thermal and RGB cameras (cell phone) to be attached side by side, resulting in a similar viewing area for the pair of lenses. Both viewing areas can be compared in Figure 32, making the difference in the image size and angle clear. The presented thermal image is from the moment when the turbine housing reached its highest temperature to facilitate the visualization of the object.

Figure 30 – Thermal camera position

Source: Author.

Although it was only necessary for one RGB image, which could be shot manually, it needed multiple thermal images, requiring an automatic shooter. Besides that, the thermal camera does not have any buttons, so it demands a code activation for any activity. Both situations are settled by using a python code that communicates with the

Figure 31 – Cameras holder

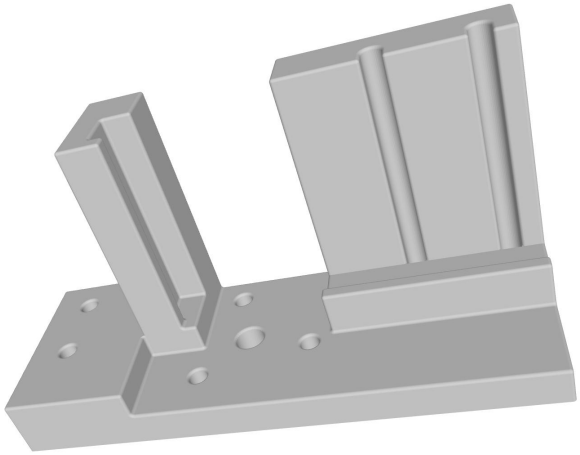

Source: Author.

Figure 32 – Viewing area of thermal and RGB camera

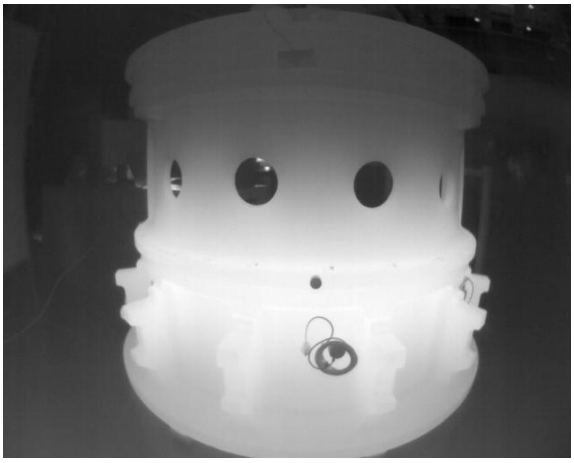

(a) Thermal

(b) RGB

Source: Author.

camera software and triggers a new photo every 5 minutes during the whole experiment. For this reason, a computer must be connected to the camera at all times. All pictures are saved locally in the computer with *numpy* format.

With all measurement equipment correctly configured and positioned, that is, the temperature is measured by sensors and the thermal camera, and the deformation of the object by the laser tracker, the experiment itself can start. For this, the first step is turning on the 9 heat pads to heat up the turbine housing. All heat pads are connected to an ESP32 and each of them is turned on individually by sending a signal using the Arduino software. Their power is not configurable. The heating process started at 9:38 a.m. on October 07, 2022, and was turned off at 12:38 p.m. on the same day. Even though there was no more heating, the measurement equipment remained on, monitoring the turbine housing until 00:43 a.m. the next day.

4.5 DATA TREATMENT

After acquiring all data from the heating and cooling process of the turbine housing, all information needs to be processed with different techniques. The first step is to take care of the cameras and images, which means that is necessary to perform a camera calibration in order to get internal information from both equipment and use it to reduce the lens distortion in the images. Then, the images with less distortion can be used to allow automatic detection of the sensors by neural network processing.

After that, the temperature captured in the thermal images must be converted from the camera signal value to Celsius. With this information, it is possible to compare the images with temperature sensor data, looking for a possible difference between the results of the different types of temperature measurement used. If it exists, it may be fixed by creating an equation for the difference. Lastly, the temperature data can go through interpolation, following a connection of temperature to the nodes of the turbine housing a 3D virtual model. All steps are important to finally perform the simulation of the experiment using the software. The simulation results can then be used for the comparative analysis between the real and virtual worlds.

The camera calibration requires a group of thermal and RGB images containing a metal chessboard. Examples of a pair of images are shown in Figure 33. The chessboard is important due to the methodology applied by the calibration routine, which detects the size of each square and performs further calculations using it. A better explanation of the camera calibration tool is in the author's mandatory internship report, a work prior to this one. As a result, the tool presents the focal length, principal point, skew, distortion, and pixel error from both cameras, together with the rotation and translation vector between them. Data from the thermal camera is presented in Table 5, from the RGB camera is in Table 6 and the extrinsic parameters from both cameras is in Table 7.

Figure 33 – Images for camera calibration

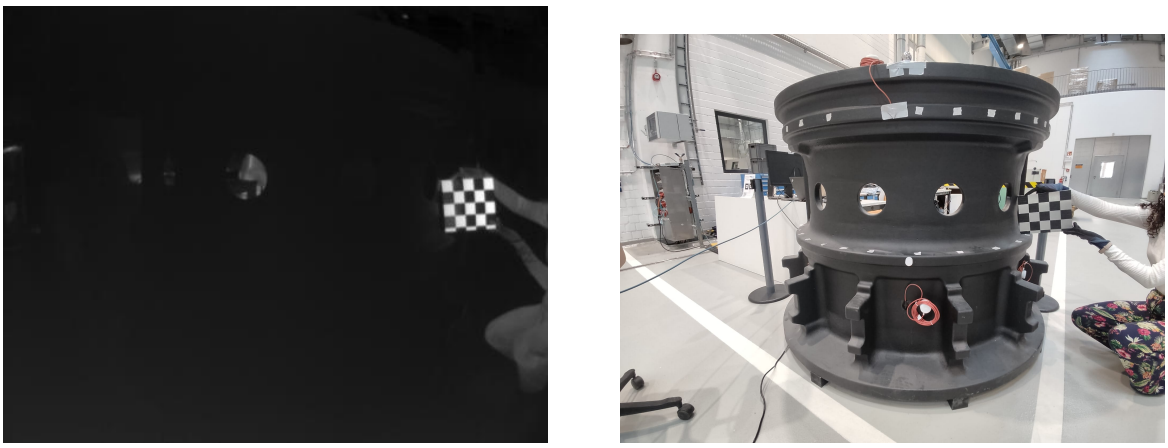

(a) Thermal (b) RGB

Source: Author.

Table 5 – Thermal camera calibration.

	Thermal
Focal Length	[493.21037 496.85938]+/-[158.42428 162.28782]
Principal point	[257.74073 103.22597]+/-[20.46013 38.12089]
Skew	[0.00000]+/-[0.00000]
Distortion	[-0.93317 0.61146 0.08137 -0.00598 0.00000]+/-[0.57939 0.83140 0.05881 0.02395 0.00000]
Pixel error	[0.43557 0.59589]

Table 6 – RGB camera calibration.

	RGB
Focal Length	[1541.03689 1565.00908]+/-[233.03823 243.07797]
Principal point	[1066.09774 850.73989]+/-[170.77724 91.98969]
Skew	[0.00000]+/-[0.00000]
Distortion	[-0.01709 -0.06727 -0.01350 0.06479 0.00000]+/-[0.10412 0.16820 0.02218 0.02739 0.00000]
Pixel error	[0.95167 1.17985]

By getting this data, the images can go through a process to reduce the deformation caused by the camera's lenses, correcting curved lines to straight ones. The result of this process is presented in Figure 34. The resultant images, together with the extrinsic parameters from both cameras, can be further explored to find a mathematical conversion of a pixel from one image to another that represents the same point in

Table 7 – Extrinsic parameters.

	Position of right camera with respect to left camera
Rotation vector	[0.08453 0.11371 -0.02286]
Translation vector	[-192.38015 40.23090 144.21075]

reality. Beyond that, the rectified images are a better fit to be analyzed by the RCNN neural network (a technique explored in the author's mandatory internship report), in an attempt to detect the positions of the sensors in the thermal images when the thermal contrast does not make them perceptible. In this particular experiment, the sensors were clearly visible, so the use of the neural network was not necessary.

Figure 34 – Result of reduction of deformation

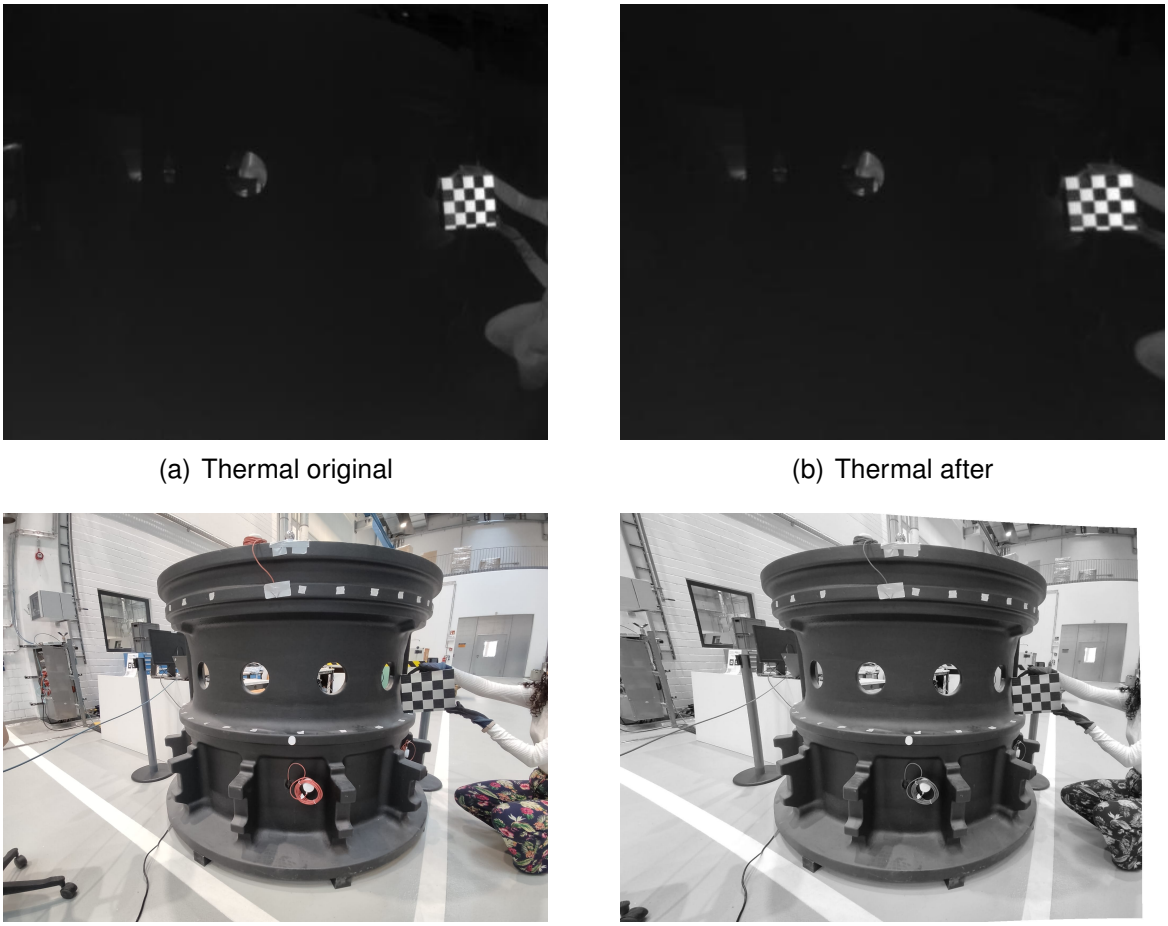

(a) Thermal original

(b) Thermal after

(c) RGB original

(d) RGB after

Source: Author.

After treating the images' distortion, the thermal images still need more processing. Initially, they are saved in *numpy* format, with a different camera signal value composing each pixel. As explained in Section 4.2.2, the camera signal is a result of temperature and radiation as the emissivity of the object. In future analyzes, it is better to use temperature in Celsius, instead of the camera signal, as a working value. For this reason, using the previously explained equations, the signal can be transformed into a temperature value by processing all images with a python script. An example of this transformation is presented in Table 8. The table contains the first 3 rows and columns of pixels from an image for both signal and temperature values. With this transformation, the images are properly treated and ready to be analyzed.

Table 8 – Camera signal and temperature values from the thermal image.

		Column 1	Column 2	Column 3
Line 1	Temperature	20.38564	20.33389	20.20438
	Signal	3141	3139	3134
Line 2	Temperature	20.35977	20.33389	20.30800
	Signal	3140	3139	3138
Line 3	Temperature	20.17845	20.48908	20.35977
	Signal	3133	3145	3140

In future analysis, it is important to have well-calibrated thermal images that contain temperature values as close as possible to reality. A significant point that must be highlighted is that thermal cameras can more truthful measure points that are positioned at 90° from the camera, vertically and horizontally, so that points located at the edges of the image are less reliable. Considering that thermography technology, such as the thermal camera, can be a source of error, a comparison between the temperature values acquired with thermography and the temperature sensor regarding the turbine housing is essential. Thus, if a significant difference really exists, the images can be calibrated so that the next steps are not influenced by this error.

In order to make this comparison, pixels from the thermal images were manually chosen next to the sensors to represent the most similar thermal point. Their positions are related to sensors 2, 3, and 5, located at the middle top, right top, and center part of the turbine housing, respectively. For better visualization, the chosen thermal points were marked with a red dot in the thermal image presented in Figure 35. For this test, all thermal images were processed.

Figure 35 – Thermal points related to sensors 2, 3 and 5.

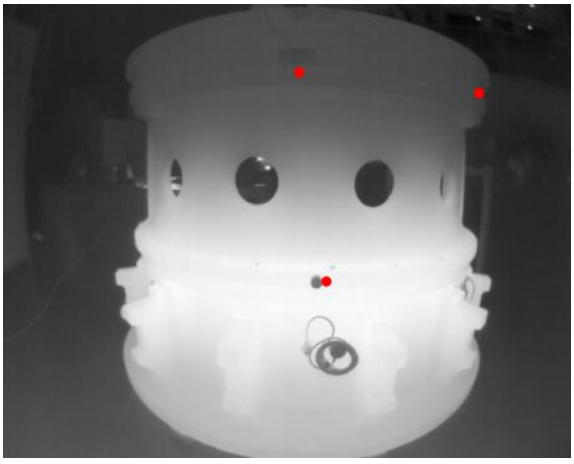

Source: Author.

The results of the comparison for all 3 sensors are presented in Figure 36. While the points close to sensors 2 and 3 only varied about 2.5℃ during the whole experiment, the sensor 5 region had a variation of about 20℃, according to the sensor's

measurements. In contrast, thermography shows a variation of 25 ℃ for sensor 5, pointing to a big difference between both pieces of equipment. The difference in temperature variation between the sensors can be explained by their positions. Sensor 2 is near the top of the object, suffering influence from the air above. Sensor 3 is located at the right corner of the object, being influenced not only by the air above but also from the side. Sensor 5, however, is in the center of the turbine, having less contact with the air, and also much closer to the heaters.

A more focused analysis of the results from point 5, due to its large temperature variation, shows that for temperatures around 40 ℃ the error is close to 5 ℃, while for lower temperatures the error decreases to nearly 2 ℃, indicating that the error between the thermography and the sensor varies with temperature, and not with time as it may seem. In order to use these results to calibrate all thermal images it is relevant to investigate if the error has a linear behavior regarding the temperature variation.

The linear regression for all 3 points was calculated using Python, specifically the *scipy* library and the *linregress* function. The results from each point can be visualized in Figure 37. The used function returns important information about the regression, such as the slope and intercept values that compose the resulting line, as well as the coefficient of determination (R^2) and $p - value$. For point 2 the linear equation is given by

$$e = 0.6239439142537991\,T - 12.44152011832755, \tag{21}$$

where e is the error and T is the temperature in Celsius, with $R^2 = 0.29422571072$ and $p - value = 1.49$. Point 3 has a linear equation of

$$e = 0.2843974138420933\,T - 4.714539754583876, \tag{22}$$

with $R^2 = 0.29403843094$ and $p - value = 1.88$. Lastly, point 5 is given by

$$e = 0.19646070797247955\,T - 2.548382030841874, \tag{23}$$

with $R^2 = 0.93392695037$ and $p - value = 0.0$.

Analyzing the distribution of error for points 2 and 3 it is possible to notice that the error is too spread through the range of temperature. In addition, point 2 shows a different standard deviation for most error data, which may be a sign that the data used cannot be trusted for the analysis in the discussion. The non-usability of this data is confirmed for the $p - value$ of both points, which pass 1, meaning that the data does not have a reliable correlation between error and temperature. Although these are not the expected result, they can be explained by the small range of variation from the temperature during the experiment. Such small ranges do not allow adequate analysis of the error behavior.

Figure 36 – Temperature comparison between sensor and thermography.

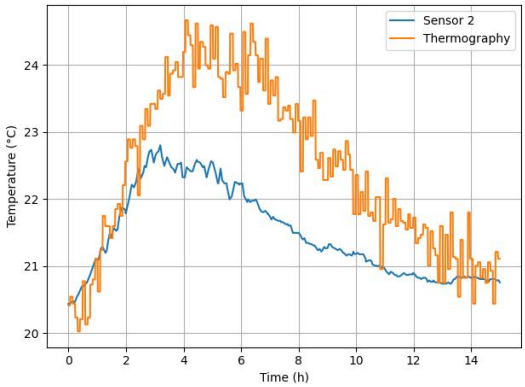

(a) Sensor 2 and thermal point

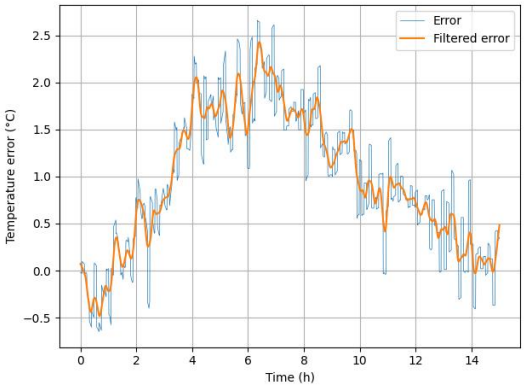

(b) Sensor 2 and thermal point error

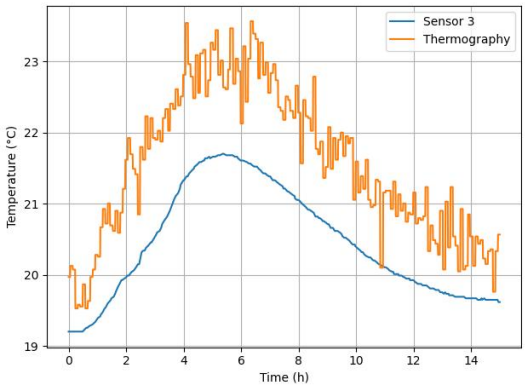

(c) Sensor 3 and thermal point

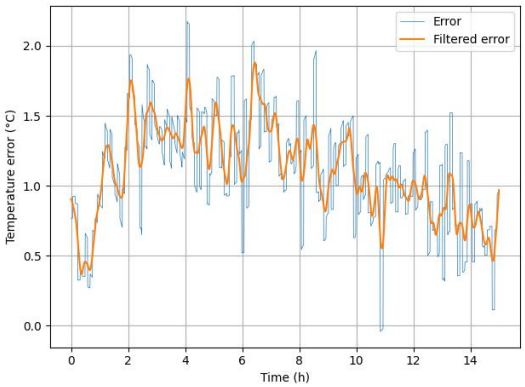

(d) Sensor 3 and thermal point error

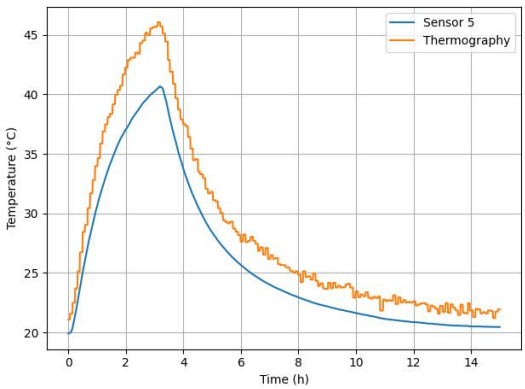

(e) Sensor 5 and thermal point

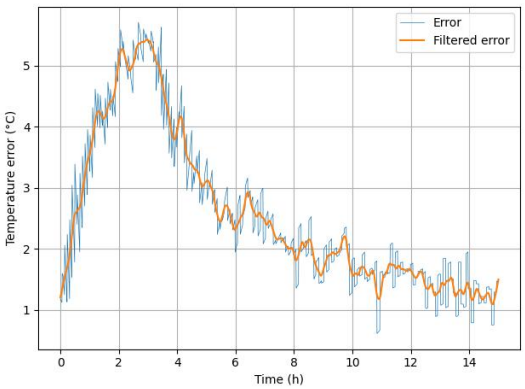

(f) Sensor 5 and thermal point error

Source: Author.

In contrast, point 5 provided a more reliable result. The $p - value$ equal to 0 indicates an existent correlation between error and temperature. This is confirmed by the coefficient of determination, which shows that the error can be predicted in 93% of cases. Since point 5 is located in the middle of the image and the turbine housing, is prone to have fewer errors related to thermal camera capture, and resulted in a usable linear regression with a great coefficient of determination, its resultant equation from

Figure 37 – Linear regression for temperature comparison error.

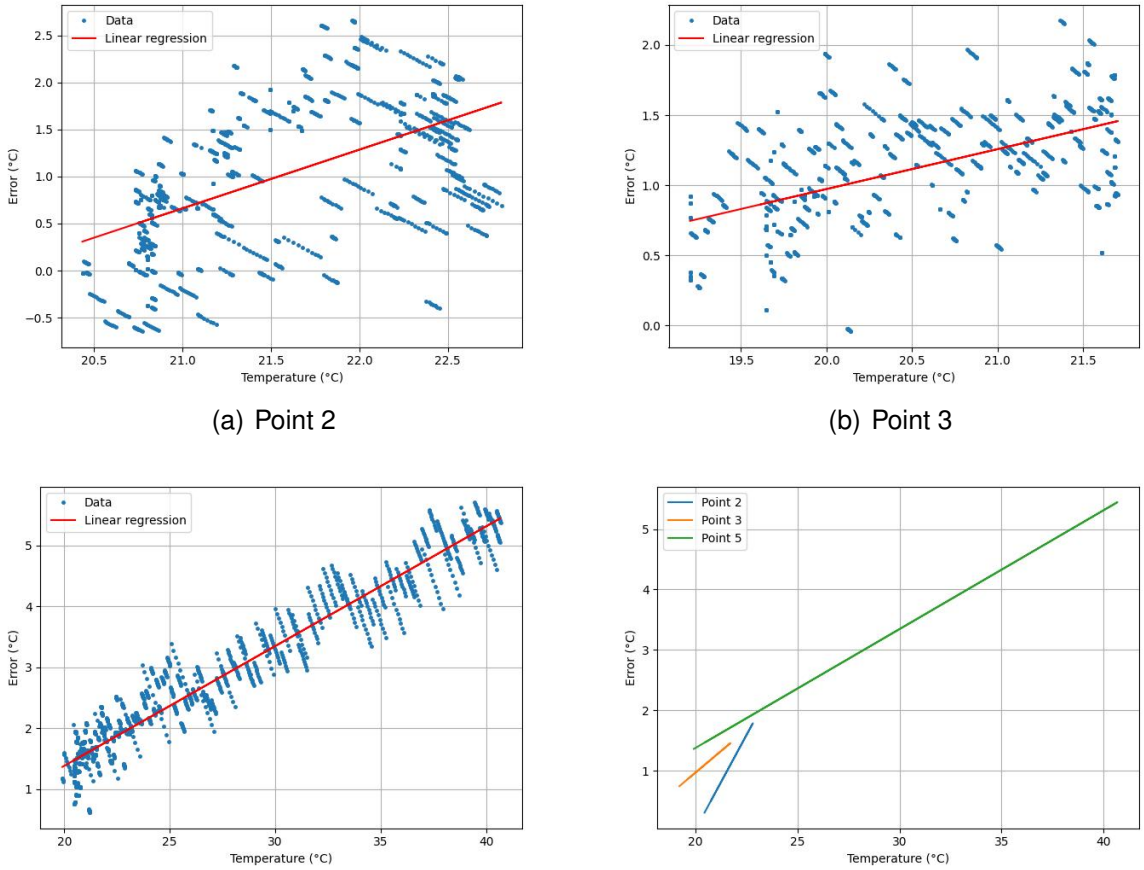

(a) Point 2

(b) Point 3

(c) Point 5

(d) All points

Source: Author.

the regression (Equation (23)) is going to be used to calibrate all temperature errors from the thermal images.

To do so a python script was created to read the image's pixel value and calculate their specific error one by one. A piece of the code is presented in sequence. Variable *img_array* represents the original image and *x* and *y* represent the pixel coordinates. Each pixel value is used to calculate its corresponding error and then the error is subtracted from the pixel itself, resulting in an image fully calibrated without temperature error in a customized manner.

```
slope = 0.19646070797247955
intercept = -2.548382030841874

new_image_array = np.zeros([512, 640])
for i in range(len(img_list)):
    img_array = np.load(img_path + img_list[i])
    for x in range(len(img_array)):
        for y in range(len(img_array[0])):
            error = (slope * img_array[x][y]) + intercept
```

```
new_image_array[x][y] = img_array[x][y] - error
```

The ability to create a connection between the 3D virtual model of a turbine housing and the temperature values from a thermal image allows the creation of a realistic virtual representation of the real turbine housing. This is made possible through the use of well-calibrated images with temperature data from the whole object. Such a virtual representation is important for use in future simulations. It allows for the analysis and prediction of the behavior and performance of the turbine housing under various conditions. By using the processed images, it is now possible to establish the necessary connection between the temperature values shown in the thermal image and the nodes in the 3D virtual model of the turbine housing.

To perform this connection, the image is attached to the virtual object using the UV-mapping tool from the Blender software. This process, known as UV mapping, involves projecting the texture of the image onto the 3D model of the virtual object. By aligning the image with the correct areas of the model, it appears as if the texture is actually applied to the surface of the object. As this experiment only contains front-view thermal images from the turbine housing, the virtual model was UV-mapped based only on its front view, so the turbine was mapped as 1 single piece, instead of 6 as presented before. The UV-map and its resulting effect can be seen in Figure 38.

Figure 38 – Real experiment UV-map.

(a) UV-map (b) Result

Source: Author.

Although the UV-mapping technique produces a visually appealing result, the mapping of the lateral parts of the object has some errors. This is because the process involves flattening the object, which can result in the center region being more reliable in terms of temperature than the lateral regions. As a result of this issue and the fact that the turbine has a symmetrical temperature distribution, only a few nodes of the turbine

will be used in the simulations. These points will serve as the input for an interpolation process to calculate the temperatures at all of the remaining nodes.

The 10 chosen nodes are represented by the orange triangles in Figure 39. Their positions are also introduced as thermal points in Figure 29. To actually obtain the respective temperature values from these nodes, a ply file containing all the connections between temperature and node must be exported from Blender and processed using a Python script, as explained at the end of Section 4.2.2.

Figure 39 – Selected points.

Source: Author.

In order to run simulations for various time steps of the experiment, it was necessary to repeat the procedure for obtaining temperature data from the object nodes using multiple images. A total of 10 images were utilized, with each one representing a time step with an interval of 1 hour, beginning at 9:38h and ending at 18:38h. In addition to the data obtained from the images, it was also necessary to collect the temperature measurements from the sensors, which were taken at the same time steps. As the internal surface of the turbine housing had its temperature measured by only four sensors that were located near the lateral edges, two points were selected in the horizontal center of the turbine, vertically aligned with the sensors. These points are depicted as yellow dots in Figure 29. The temperature of these points was determined by the average temperature of their respective aligned sensors.

The coordinates and temperatures from all 10 thermal points, 13 temperature sensors, and 2 additional points, a total of 25 different regions of the turbine housing, can be used as input for interpolating temperature values for all remaining nodes of the virtual object. The distance from each node was first calculated using Dijkstra's algorithm, and then the interpolation was carried out using the ordinary kriging algorithm. Both algorithms were implemented in the Python programming language. Once again the procedure was conducted for all time steps and their results can be seen in Figure 40, where the temperature distribution is identified by colors, with blue as cold

and yellow as hot.

Figure 40 – Interpolation results for 10 time steps

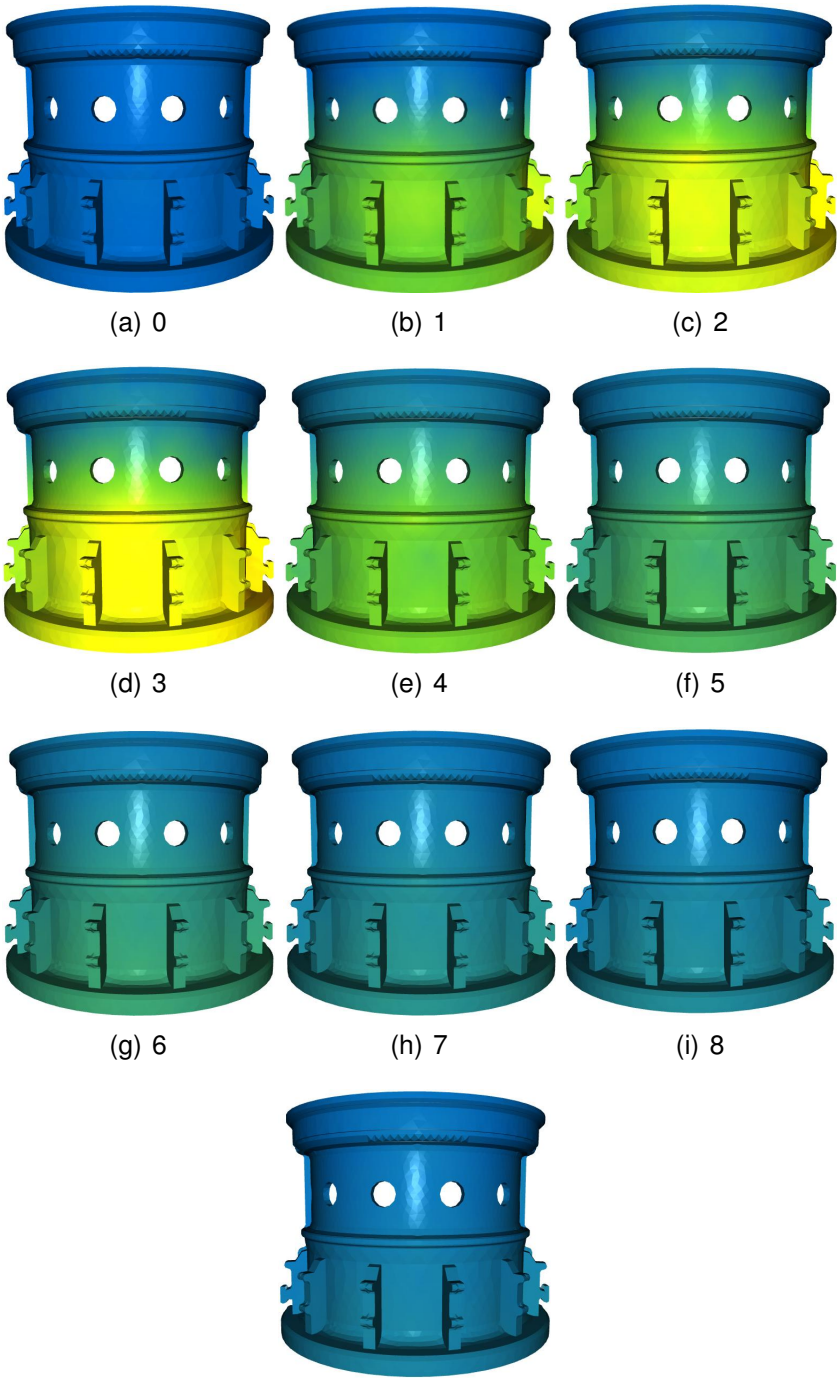

(a) 0 (b) 1 (c) 2

(d) 3 (e) 4 (f) 5

(g) 6 (h) 7 (i) 8

(j) 9

Following completion of the outlined steps, each node in the virtual turbine housing has been assigned a different temperature value for all time steps. This data can now be used as input for simulating the heating and cooling process of the turbine housing. The goal of the simulation is to get data regarding the deformation of the turbine housing material caused by the heterogeneous change of temperature. To do so, the virtual object, along with its physical characteristics and constraints, must be imported

into a finite element method (FEM) simulation software. Later on this result is going to be compared with the real experiment data, which still needs to be processed.

After setting the material's mechanical and thermal properties, and the physical constraint to prevent the object from expanding downward, since it is resting on the ground, the temperature of each node is passed to the configuration file using a python script, as explained in Section 4.2.5.1. Then, the simulation is performed using the *Calculix* tool, resulting in a calculation of the deformation and stress suffered by the object due to the temperature.

4.6 DEFORMATION ANALYZES AND RESULTS

With the simulation already performed, the resulting data can be analyzed for a better understanding of the object's deformation at each time step. Furthermore, the real experiment data from the distance measurement of the SMRs by the laser tracker should also be analyzed for different time steps. Finally, data concerning the deformations suffered by the object, acquired from the real measurements and from the simulations, can be compared.

Starting with the simulation, the FreeCAD results from each time step needs to be exported as VTK files, which are then processed by a Python script that reorganize the file in columns of data containing the coordinates, displacement and temperature from each node. This data can be processed to calculate the distance between 2 points, resulting in the deformation suffered by the object regarding the chosen points. For this project, 4 measurement lines were set up: an horizontal top line, which represents the distance and deformation of SMRs 0 and 2; an horizontal middle line, for SMRs 3 and 5; a vertical left line, for SMRs 0 and 5; and a vertical right line, for SMRs 2 and 3.

Coordinates from specific nodes that are correlated to the SMRs position 0, 2, 3 and 5, were processed, and the distance between each pair of SMRs were estimated using the euclidean norm. The deformation was calculated by subtracting the original distance between the points in the neutral object from the distance value after the simulation with a higher temperature.

For the real experiment, where the points positions were measured by the laser tracker, the procedure is similar. The data from the experiment was sent to a database containing the exact time of measurement and coordinates from the SMRs. Since the laser tracker measured all 8 SMRs in a loop, their data were mixed in a single file. By using the SMRs original coordinates, it was possible to filter the data from the four chosen SMRs and calculate the distance and deformation from the SMRs pairs using the same methodology as used for the simulation results.

Deformation values from simulation and real experiment are presented in Figure 41. It is noticeable a measurement error by the laser tracker for the vertical right line, which must not be considered in future analyzes. Analyzing the measurements

maximum values, the horizontal top line has a simulation error of 45%, the horizontal middle an error of 26.3%, the vertical left an error of 25.7% and the vertical right an error of 16.4%, resulting in an average error of 28.35%.

Figure 41 – Measurement lines deformation comparison with CTE=11.1mm/mm/K

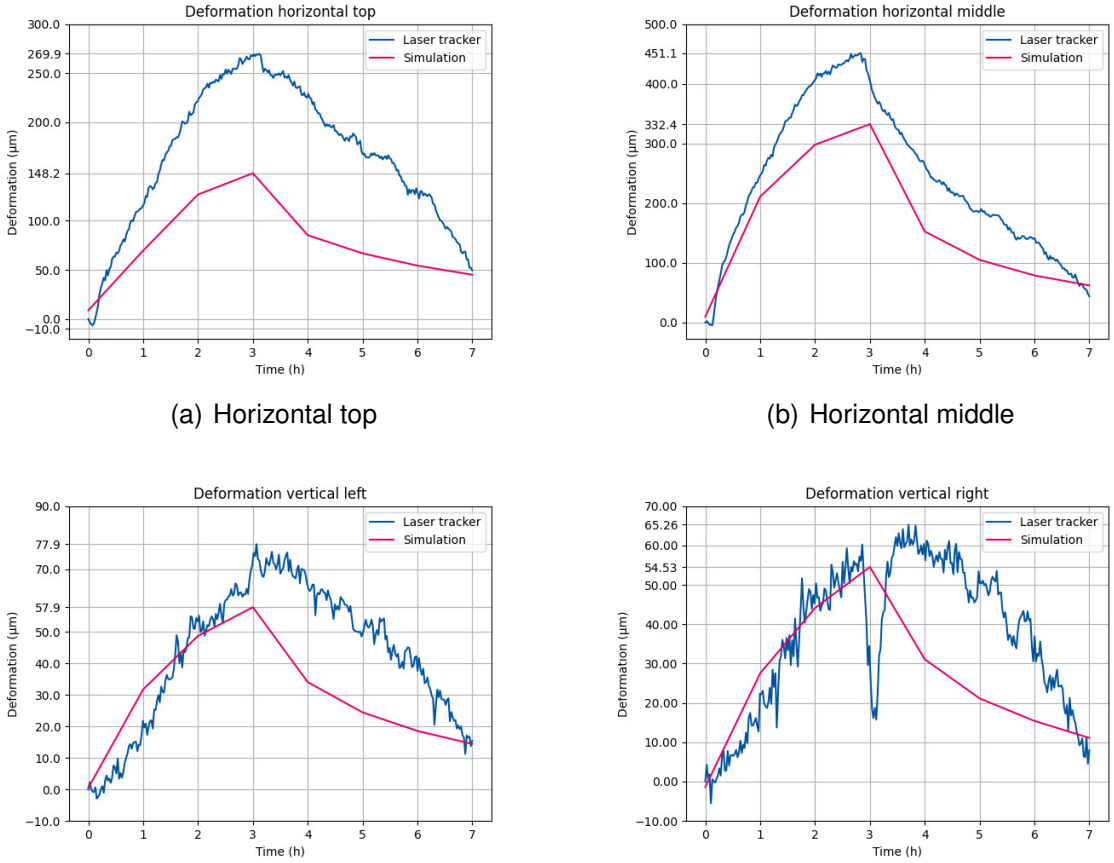

(a) Horizontal top

(b) Horizontal middle

(c) Vertical left

(d) Vertical right

Source: Author.

With a coefficient of thermal expansion of 11.1mm/mm/K, the linear thermal expansion (LTE) can be calculated for the different temperatures of the turbine points in the experiment. The LTE for all 4 measurement lines is presented in Figure 42. It is important to consider that the LTE was calculated based on the temperature from the closest temperatures sensors from each SMRs, resulting in 2 sensors per line and a focus on the region temperature.

In the presented figure is possible to notice that the LTE for the horizontal top, a region where the temperature increases very little during the experiment, is close to 50μm, which is a small value if compared with the real measurement. This can be explained by the influence that the deformation of the horizontal middle line has on the horizontal top line in reality, since once the middle of the turbine expands, the top also inherits some of this expansion. This behavior is not considered in LTE calculations.

Figure 42 – LTE of the measurement lines with CTE=11.1mm/mm/K

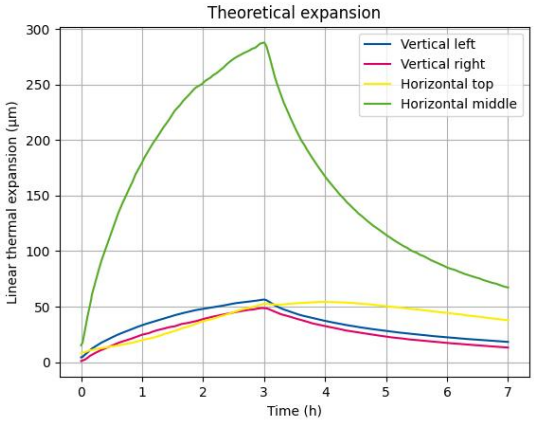

Source: Author.

On the other hand, examining the LTE for the other lines, it shows a value closer to the real measurement, but still, there is an error of 27.4%, 25.5% and 36.2% for the vertical left, vertical right and horizontal middle lines, respectively, over the real measurement. Considering that the theoretical and simulated deformation are always smaller than the one measured by the laser tracker, a possible source of error is the used coefficient of thermal (CTE) expansion. Because of this indication, and the empirical nature of that value, new deformations were calculated using a CTE 30% bigger than the original, with a value of 14.4mm/mm/K.

After running new simulations with the increased CTE, the deformations were processed and the new results are presented in Figure 43. Now, the errors between real and simulated data are smaller. The horizontal top line still presents the greater error from all 4 measurement lines with a value of 31%, which is expected since it suffers with influence from the whole object expansion, becoming the most difficult one to predict. Even so, it had an improvement of 31.11% over the error seen in the previous analysis.

The other 3 lines have a even better result. The horizontal middle, vertical left and vertical right lines have an error of 11.33%, 0.13% and 13.9%, respectively. When compared with the previous data, it means a improvement of 56.92%, 99.49% and 15.24%. Besides, all theoretical linear thermal expansions increased. Their results are presented in Figure 44. The LTE error over the real measurement is 17.24%, 5.99% and 2.97% for the horizontal middle, vertical left and vertical right measurement lines, showing a great improvement over the previous data. The average error relative to the linear temperature expansion theoretical values is 8.73%.

Although the increase in the value of the used CTE resulted in improvements, there are still significant errors that need to be addressed. The deformation measurements play a significant role in the research field, but they are relatively insignificant on a global scale. As a result, these measurements can be susceptible to a variety

Figure 43 – Measurement lines deformation comparison with CTE=14.4mm/mm/K

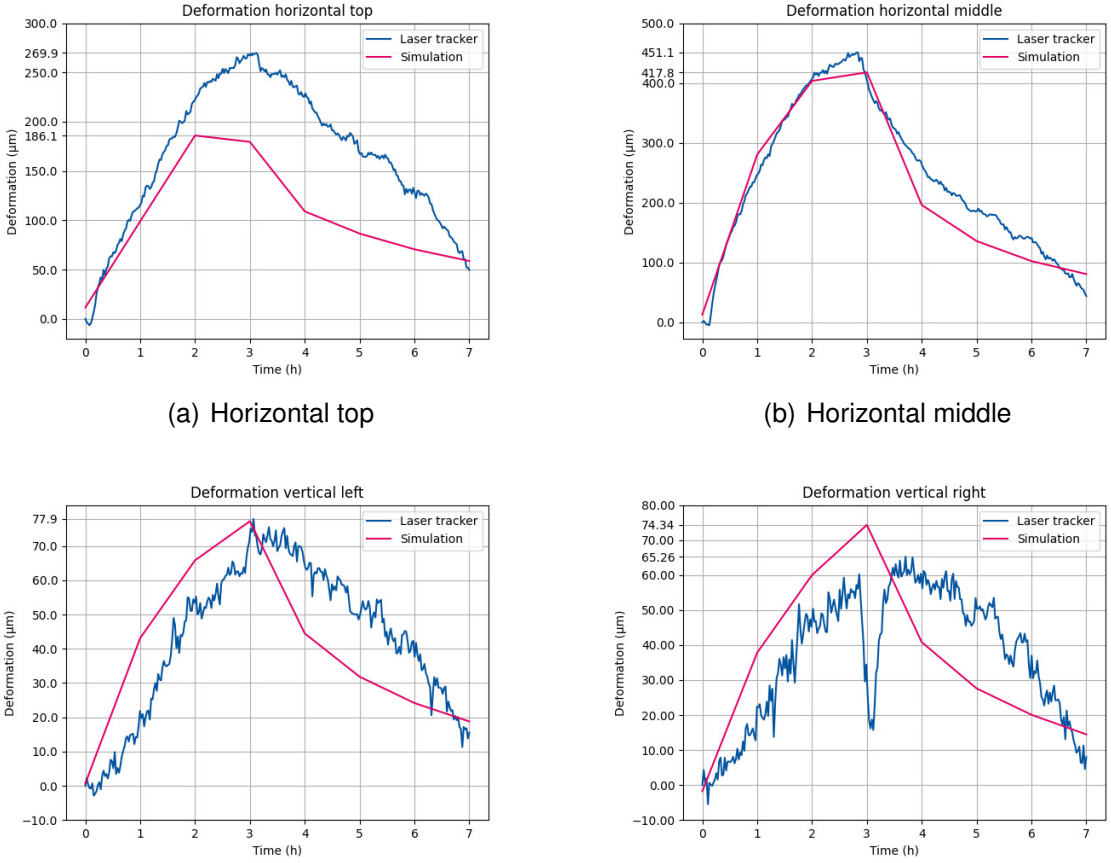

(a) Horizontal top

(b) Horizontal middle

(c) Vertical left

(d) Vertical right

Source: Author.

Figure 44 – LTE of the measurement lines with CTE=14.4mm/mm/K

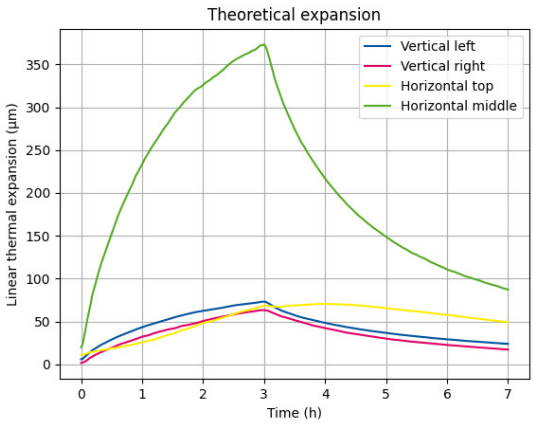

Source: Author.

of factors that can lead to errors in measurement and prediction. The main possible source of errors are presented in Figure 45.

Trying to quantify a possible influence from the interpolation over the results,

Figure 45 – Possible sources of error prediction

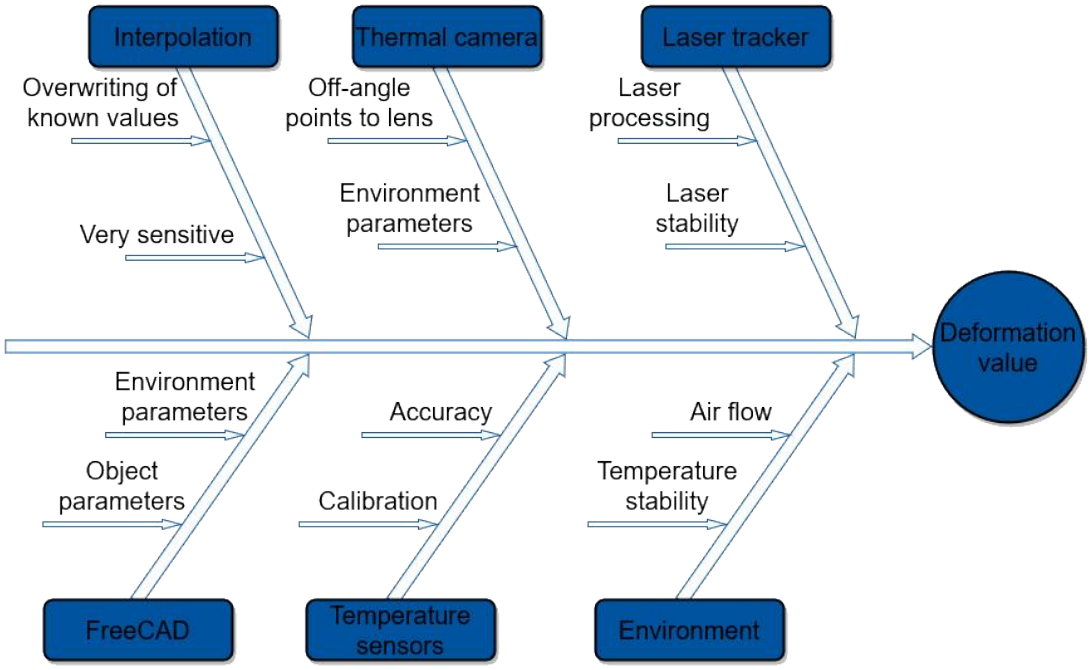

Source: Author.

an analyze of the overwritten temperature value was performed. Table 9 shows the temperature error for the main sensors used in this experiment, such as 10, 11, 12 and 13, correspondent to top left, top right, middle left and middle right positions, respectively. It is possible to observe that the interpolation procedure is underestimating the values for middle region when the turbine is heating (time step 2, 3 and 4), which are the warmest region. The average error of 0.96℃ causes a difference in thermal expansion of 14.92μm for a CTE of 11.1mm/mm/K and 19.35μm for a CTE of 14.4mm/mm/K.

Table 9 – Interpolation error in Celsius.

Time step	Top left	Middle left	Top right	Middle right
1	-0.198886	-0.520336	-0.164353	-0.322214
2	0.0221402	-1.1691	0.00745291	-0.724156
3	0.0658477	-1.18892	0.0843719	-0.723558
4	0.0726119	-1.20331	0.0824525	-0.743671
5	-0.0870665	-0.615113	-0.041178	-0.424975
6	-0.139723	-0.555234	-0.0940854	-0.331331
7	-0.159153	-0.531206	-0.110312	-0.291542
8	-0.167375	-0.528605	-0.11855	-0.305493
9	-0.177499	-0.53452	-0.121504	-0.304865
10	-0.18066	-0.530627	-0.124129	-0.301096

In addition to the impact of interpolation on the results, there are potential sources of error, as depicted in the diagram, that may influence the result. To further investigate these sources of error, the institute conducted a parallel study on the stability and precision of the laser tracking equipment. The laser tracking device was

utilized to measure the turbine housing for a duration of 24 hours, with no heat applied. The results of the experiment revealed a deformation of the object, indicating that it contracted over time. Certain peaks of deformation observed in the data suggest a possible influence of temperature fluctuations on the factory floor during the day. However, the data set also suggests that the laser tracker may lose its accuracy when used in a loop, which may not be the case when used with a single stationary object.

The value of the average percentage error obtained is considered satisfactory, not only because of the possible sources of error that should be explored, but mainly because this project was the first work at the institute that pursued the development and implementation of a framework for predicting the thermoelastic deformation of parts on a large scale following the methodology presented.

It is important to note that there may be other sources of error that should be explored in future studies. Further research is necessary to fully understand and address these potential sources of error. This will enable more accurate and reliable results to be obtained and may provide insight into how to improve the measurement and analysis process. By exploring these other sources of error, we can ensure that the results are as accurate and reliable as possible and that any potential issues are identified and addressed.

5 CONCLUSION

Errors in the production of large-scale parts can result in a decrease in product quality and efficiency, as well as a threat to the product safety. Such errors are often linked to temperature changes in the environment or in the object itself, which result in expansion of the material due to its thermoelastic behavior. The increase in size, even if in the order of micrometers, is considered high in a manufacturing process, as the error tolerance is small for large parts, as regulated by ISO 2768. With this, there is an urgency for a technology that can help in understanding the changes that occur in large objects.

Considering the influence that a small change in temperature can have over a large scale workpiece production, experiments were conducted in which a large turbine housing was forced heated in order to acquire data concerning the temperature and deformation of the object while the temperature was not stable or homogeneous. The data was collected using multiple measurement equipment, such as temperature sensors, a thermal camera and a laser tracker.

All data required treatment and processing so it could be used in FEM simulations with the objective to predict the object deformation in a range of temperature. A comparison between simulation results and real measurements from the experiment was performed. Four lines of deformation were studied and the simulator was able to reach a deformation value with an average error of 28.35% over the real measurements.

Analysis showed that the simulator provides a deformation outcome with a pattern similar to the real behavior of the turbine considering the time line, but with a significant error in value. Results closer to reality could be achieved by increasing the value of the CTE, i.e. by empirically changing the physical properties of the object, which improved the result in 31.11%. The result is considered suitable and sufficient for the proposed and implemented methodology, specially considering the innovative attempt to implement a prediction technology for the deformation of large workpieces for the first time in WZL.

It was made clear that all the multiple steps required to reach the simulation point, as well as the used equipment, are very susceptible to errors, and some of them are so sensible that small changes in temperatures value results in great impact on the object's final deformation value. Since all those sources of error can accumulate, different avenues for future work remain open. Topics such as interpolation parameters, angle between camera lens and object, laser-tracker stability in routines, physical parameters of the object and the environment, accuracy of the temperature sensors and environmental temperature stability remain as suggestions for further research.

REFERENCES

AUTOMATION TECHNOLOGY. **IRSX Operating Manual: IRSX-I336, IRSX-I640**. [S.l.: s.n.]. Available from: https://www.stemmer-imaging.com/media/uploads/cameras/at/14/149469-AT-IRSX-Series-Manual.pdf.

BARNES, Randal. **Variogram Tutorial**. [S.l.: s.n.]. Available from: http://www.goldensoftware.com/variogramTutorial.pdf.

BIGLINO, Giovanni; CAPELLI, Claudio; KONIORDOU, Despina; DI ROBERTSHAW; LEAVER, Lindsay-Kay; SCHIEVANO, Silvia; TAYLOR, Andrew M.; WRAY, Jo. Use of 3D models of congenital heart disease as an education tool for cardiac nurses. **Congenital heart disease**, v. 12, n. 1, p. 113–118, 2017. DOI: 10.1111/chd.12414.

BLENDER 3.3 Reference Manual. 3.3. ed. [S.l.: s.n.]. Available from: https://docs.blender.org/manual/en/3.3/index.html.

BLENDER ONLINE COMMUNITY. **Blender - a 3D modelling and rendering package**. [S.l.: s.n.], 2018. Available from: http://www.blender.org.

CARUSO, C.; QUARTA, F. Interpolation methods comparison. **Computers & Mathematics with Applications**, v. 35, n. 12, p. 109–126, 1998. ISSN 08981221. DOI: 10.1016/S0898-1221(98)00101-1.

CHEN, Zhiqin; YIN, Kangxue; FIDLER, Sanja. **AUV-Net: Learning Aligned UV Maps for Texture Transfer and Synthesis**. [S.l.]: arXiv, 2022. DOI: 10.48550/arXiv.2204.03105.

CHEN, Yi-zhou; SHEN, Shi-fei; CHEN, Tao; YANG, Rui. Path Optimization Study for Vehicles Evacuation based on Dijkstra Algorithm. **Procedia Engineering**, v. 71, p. 159–165, 2014. ISSN 18777058. DOI: 10.1016/j.proeng.2014.04.023.

CHEOK, Geraldine; SAIDI, Kamel. Robotics to benefit from 3D vision standard. n. 100, p. 26–29, 2020.

CHUNG, Sang Yong; VENKATRAMANAN, S.; ELZAIN, Hussam Eldin; SELVAM, S.; PRASANNA, M. V. Supplement of Missing Data in Groundwater-Level Variations of Peak Type Using Geostatistical Methods. In: VENKATRAMANAN, Senapathi; VISWANATHAN PRASANNA, Mohan; YONG CHUNG, Sang (Eds.). **GIS and**

Geostatistical Techniques for Groundwater Science. [S.l.]: Elsevier, 2019. P. 33–41. ISBN 9780128154137. DOI: 10.1016/B978-0-12-815413-7.00004-3.

COLUMBIA. **Kriging Interpolation**. [S.l.: s.n.]. Available from: https://www.publichealth.columbia.edu/research/population-health-methods/kriging-interpolation.

CONNOR, J. J.; BREBBIA, C. A. **Finite element techniques for fluid flow**. London: Newnes-Butterworths, 1976. ISBN 0408001763.

CORREIA, Pedro. **Modelação e Estimação: Uma introdução à geoestatística**. [S.l.: s.n.], 2010.

DÉROBERT, Xavier; BALAYSSAC, Jean-Paul; SBARTAÏ, Zoubir Mehdi; DUMOULIN, Jean. Electromagnetic Methods. In: NON-DESTRUCTIVE Testing and Evaluation of Civil Engineering Structures. [S.l.]: Elsevier, 2018. P. 87–137. ISBN 9781785482298. DOI: 10.1016/B978-1-78548-229-8.50003-0.

DIJKSTRA, E. W. A note on two problems in connexion with graphs. **Numerische Mathematik**, v. 1, n. 1, p. 269–271, 1959. ISSN 0029-599X. DOI: 10.1007/BF01386390.

DS18B20: Programmable Resolution 1-Wire Digital Thermometer. [S.l.: s.n.], 2019. Available from: www.maximintegrated.com.

FADERO, Patrick Eniola; SHAH, Mahir. Three dimensional (3D) modelling and surgical planning in trauma and orthopaedics. **The surgeon : journal of the Royal Colleges of Surgeons of Edinburgh and Ireland**, v. 12, n. 6, p. 328–333, 2014. ISSN 1479-666X. DOI: 10.1016/j.surge.2014.03.008.

FENG, Kang; ZHONG-CI, Shi. **Mathematical Theory of Elastic Structures**. Cham: Springer International Publishing, 1996. ISBN 9783662032862. DOI: 10.1007/978-3-662-03286-2.

GASS, Saul I.; FU, Michael C. **Encyclopedia of Operations Research and Management Science**. Boston, MA: Springer US, 2013. ISBN 978-1-4419-1137-7. DOI: 10.1007/978-1-4419-1153-7.

GEUZAINE, Christophe; REMACLE, Jean-François. **Gmsh: A 3-D finite element mesh generator with built-in pre- and post-processing facilities**. International Journal for Numerical Methods in Engineering: [s.n.], 2009.

GRIEVES, Michael; VICKERS, John. Digital Twin: Mitigating Unpredictable, Undesirable Emergent Behavior in Complex Systems. In: KAHLEN, Franz-Josef; FLUMERFELT, Shannon; ALVES, Anabela (Eds.). **Transdisciplinary Perspectives on Complex Systems**. Cham: Springer International Publishing, 2017. P. 85–113. ISBN 978-3-319-38754-3. DOI: 10.1007/978-3-319-38756-7{\textunderscore}4.

IEEE. **The Advantages of the Finite Element Method**. [S.l.: s.n.]. Available from: https://innovationatwork.ieee.org/the-advantages-of-fem/.

JAMES, J. D.; SPITTLE, J. A.; BROWN, S. G. R.; EVANS, R. W. A review of measurement techniques for the thermal expansion coefficient of metals and alloys at elevated temperatures. **Measurement Science and Technology**, v. 12, n. 3, r1–r15, 2001. ISSN 0957-0233. DOI: 10.1088/0957-0233/12/3/201.

JIN, Jian-Ming. **The Finite Element Method in Electromagnetics**. 3. Auflage. New York, NY: John Wiley & Sons, 2015. ISBN 9781118842027.

KAVEH, A. **Computational Structural Analysis and Finite Element Methods**. 1st ed. 2014. Cham: Springer International Publishing and Imprint: Springer, 2014. ISBN 9783319029641.

KONRAD, Janusz; WANG, Meng; ISHWAR, Prakash. 2D-to-3D image conversion by learning depth from examples. In: COMPUTER Society Conference on Computer Vision and Pattern Recognition Workshops. [S.l.]: IEEE, 2012. P. 16–22. DOI: 10.1109/CVPRW.2012.6238903.

KRASIL'NIKOV, N. N.; KRASIL'NIKOVA, O. I. Method of converting a 2D image into a stereoscopic 3D image. **Journal of Optical Technology**, v. 81, n. 2, p. 68, 2014. ISSN 1070-9762. DOI: 10.1364/JOT.81.000068.

KRIGE, D. G. A Review of the Development of Geostatistics in South Africa. In: GUARASCIO, Massimo; DAVID, Michel; HUIJBREGTS, Charles (Eds.). **Advanced Geostatistics in the Mining Industry**. Dordrecht: Springer Netherlands, 1976. P. 279–293. ISBN 978-94-010-1472-4. DOI: 10.1007/978-94-010-1470-0{\textunderscore}17.

LAM, Nina Siu-Ngan. Spatial Interpolation Methods: A Review. **The American Cartographer**, v. 10, n. 2, p. 129–150, 1983. ISSN 0094-1689. DOI: 10.1559/152304083783914958.

LAPERRIÈRE, Luc; REINHART, Gunther. **CIRP Encyclopedia of Production Engineering**. Berlin, Heidelberg: Springer Berlin Heidelberg, 2014. ISBN 978-3-642-20616-0. DOI: 10.1007/978-3-642-20617-7.

LEWIS, Roland W. **The Finite element method in heat transfer analysis**. Chichester: Wiley, 1996. ISBN 9780471943624.

MAURICE JAMES PUTTOCK. LARGE - SCALE METROLOGY. **Gen Assem of CIRP, 28th, Manuf Technol**, v. 27, n. 1, p. 351–356, 1978. Available from: https://www.scopus.com/record/display.uri?eid=2-s2.0-0018106891&origin=inward.

MOLLEDA, Julio; USAMENTIAGA, Rubén; GARCÍA, Daniel F.; BULNES, Francisco G.; ESPINA, Adrián; DIEYE, Bassiru; SMITH, Lyndon N. An improved 3D imaging system for dimensional quality inspection of rolled products in the metal industry. **Computers in Industry**, v. 64, n. 9, p. 1186–1200, 2013. ISSN 01663615. DOI: 10.1016/j.compind.2013.05.002.

MURATA, H.; MORI, Y.; YAMASHITA, S.; MAENAKA, A.; OKADA, S.; OYAMADA, K.; KISHIMOTO, S. 32.2: A Real-Time 2-D to 3-D Image Conversion Technique Using Computed Image Depth. **SID Symposium Digest of Technical Papers**, v. 29, n. 1, p. 919, 1998. ISSN 0097-966X. DOI: 10.1889/1.1833914.

OECHSLE, Michael; MESCHEDER, Lars; NIEMEYER, Michael; STRAUSS, Thilo; GEIGER, Andreas. **Texture Fields: Learning Texture Representations in Function Space**. [S.l.]: arXiv, 2019. DOI: 10.48550/arXiv.1905.07259.

OLIVER, Margaret A.; WEBSTER, Richard (Eds.). **Basic Steps in Geostatistics: The Variogram and Kriging**. Cham: Springer International Publishing, 2015. (SpringerBriefs in agriculture). ISBN 978-3-319-15864-8. DOI: 10.1007/978-3-319-15865-5.

PORANNE, Roi; TARINI, Marco; HUBER, Sandro; PANOZZO, Daniele; SORKINE-HORNUNG, Olga. Autocuts: Simultaneous Distortion and Cut Optimization for UV Mapping. **ACM Transactions on Graphics**, v. 36, n. 6, p. 1–11, 2017. ISSN 0730-0301. DOI: 10.1145/3130800.3130845.

RADIAN 3D Laser Tracker Series. [S.l.: s.n.], 2022. Available from: https://apimetrology.com/wp-content/uploads/2022/04/API_Tracker_Brochure_2022-EN.pdf.

ROMANO, J. M.; KUCHENBECKER, K. J. Creating Realistic Virtual Textures from Contact Acceleration Data. **IEEE transactions on haptics**, v. 5, n. 2, p. 109–119, 2012. ISSN 1939-1412. DOI: 10.1109/TOH.2011.38.

SAMPAIO, Alcínia Z.; FERREIRA, Miguel M.; ROSÁRIO, Daniel P.; MARTINS, Octávio P. 3D and VR models in Civil Engineering education: Construction, rehabilitation and maintenance. **Automation in Construction**, v. 19, n. 7, p. 819–828, 2010. ISSN 09265805. DOI: 10.1016/j.autcon.2010.05.006.

SCHMITT, R. H. et al. Advances in Large-Scale Metrology – Review and future trends. **CIRP Annals**, v. 65, n. 2, p. 643–665, 2016. ISSN 00078506. DOI: 10.1016/j.cirp.2016.05.002.

SHEPPARD, William Fleetwood. **Encyclopædia Britannica: Interpolation**. 11. ed. West Bengal Public Library: University Press, Cambridge, 1910. v. 14.

SIEMENS. **Digital Twin**. [S.l.: s.n.]. Available from: https://www.plm.automation.siemens.com/global/en/our-story/glossary/digital-twin/24465.

STANDARDIZATION, International Organization for. **General Tolerances: Tolerances for Linear and Angular Dimensions Without Individual Tolerance Indications**. [S.l.]: International Organization for Standardization, 1989.

STEFFENSEN, J. F. **Interpolation**. 2nd ed. Mineola N.Y.: Dover Publications, 2006. ISBN 0486450090.

SUN, Yongbin; LIU, Ziwei; WANG, Yue; SARMA, Sanjay E. **Im2Avatar: Colorful 3D Reconstruction from a Single Image**. [S.l.]: arXiv, 2018. DOI: 10.48550/arXiv.1804.06375.

TECHNI TOOL. **IR Thermography - How It Works?** [S.l.: s.n.], 2022.

TKÁČOVÁ, Mária; HUDÁK, Radovan; FOFFOVÁ, Patrıcia; ŽIVČÁK, Jozef. An importance of camera–subject distance and angle in musculoskeletal applications of

medical thermography. **Acta Electrotechnica et Informatica**, Citeseer, v. 10, n. 2, p. 57–60, 2010.

WACKERNAGEL, Hans. **Multivariate Geostatistics: An Introduction with Applications**. Second, Completely Revised Edition. Berlin, Heidelberg: Springer Berlin Heidelberg, 1998. ISBN 978-3-662-03550-4.

WANG, Huijuan; YU, Yuan; YUAN, Quanbo. Application of Dijkstra algorithm in robot path-planning. In: 2011 Second International Conference on Mechanic Automation and Control Engineering. [S.l.]: IEEE, 2011. P. 1067–1069. DOI: 10.1109/MACE.2011.5987118.

WANG, Jun; GU, Dongxiao; YU, Zeyun; TAN, Changbai; ZHOU, Laishui. A framework for 3D model reconstruction in reverse engineering. **Computers & Industrial Engineering**, v. 63, n. 4, p. 1189–1200, 2012. ISSN 03608352. DOI: 10.1016/j.cie.2012.07.009.